Geophysical Journal International

Centroid moment tensor inversions of offshore earthquakes using a three-dimensional velocity structure model: Slip distributions on the plate boundary along the Nankai Trough

Journal:	*Geophysical Journal International*
Manuscript ID	GJI-19-1048
Manuscript Type:	Research Paper
Date Submitted by the Author:	17-Nov-2019
Complete List of Authors:	Takemura, Shunsuke; University of Tokyo Earthquake Research Institute Okuwaki, Ryo; University of Tsukuba, Faculty of Life and Environmental Sciences Kubota, Tatsuya; Bosai Kagaku Gijutsu Kenkyujo Shiomi, Katsuhiko; National Research Institute for Earth Science and Disaster Prevention, Earthquake Research Dep. Kimura, Takeshi; Bosai Kagaku Gijutsu Kenkyujo Noda, Akemi; Bosai Kagaku Gijutsu Kenkyujo, Earthquake and Tsunami Research Department
Keywords:	Computational seismology < SEISMOLOGY, Earthquake ground motions < SEISMOLOGY, Earthquake source observations < SEISMOLOGY, Seismicity and tectonics < SEISMOLOGY, Wave propagation < SEISMOLOGY

Centroid moment tensor inversions of offshore earthquakes using a three-dimensional velocity structure model: Slip distributions on the plate boundary along the Nankai Trough

Authors

Shunsuke TAKEMURA[1*], Ryo OKUWAKI[2], Tatsuya KUBOTA[3], Katsuhiko SHIOMI[3] Takeshi KIMURA[3], Akemi NODA[4]

[1]Earthqukae Research Institute, the University of Tokyo, 1-1-1 Yayoi, Bunkyo-ku, Tokyo, 113-0032, Japan

[2]Faculty of Life and Environmental Sciences, University of Tsukuba, 1-1-1 Tennodai, Tsukuba 305-8572, Japan.

[3]Network Center for Earthquake, Tsunami and Volcano, National Research Institute for Earth Science and Disaster Resilience, 3-1 Tennodai, Tsukuba, Ibaraki, 305-0006, Japan.

[4]Earthquake and Tsunami Research Division, National Research Institute for Earth Science and Disaster Resilience, 3-1 Tennodai, Tsukuba, Ibaraki, 305-0006, Japan.

Running Title

3D CMT inversion along the Nankai Trough

Corresponding Author

Shunsuke Takemura

E-mail: shunsuke@eri.u-tokyo.ac.jp

Phone: +81 3-5841-5689

Summary

Due to complex three-dimensional (3D) heterogeneous structures, conventional one-dimensional (1D) analysis techniques using onshore seismograms can yield incorrect estimation of earthquake source parameters, especially dip angles and centroid depths of offshore earthquakes. Combining long-term onshore seismic observations and numerical simulations of seismic wave propagation in a 3D model, we conducted centroid moment tensor (CMT) inversions of earthquakes along the Nankai Trough between April 2004 and August 2019 to evaluate decade-scale seismicity. Green's functions for CMT inversions of earthquakes with moment magnitudes of 4.3–6.5 were evaluated using finite-difference method simulations of seismic wave propagation in the regional 3D velocity structure model. Our CMT solutions were generally better than those in the catalogue based on regional 1D analysis, especially for offshore earthquakes. By introducing the 3D structures of the low-velocity accretionary prism and the Philippine Sea Plate, dip angles and centroid depths for offshore earthquakes were well-constrained. Our 3D CMT catalogue and published slow earthquake catalogues depicted spatial distributions of slip behaviours on the plate boundary along the Nankai Trough. The regular and slow interplate earthquakes were separately distributed, with these distributions reflecting the heterogeneous distribution of effective strengths along the Nankai Trough plate boundary. By comparing the spatial distribution of seismic slip on the plate boundary with the slip-deficit rate distribution, regions with strong coupling were clearly identified.

Keywords:

Nankai Trough, seismicity, centroid moment tensor inversion, heterogeneous structure, finite-difference method

1. Introduction

The earthquake focal mechanism is one of the most important parameters characterising earthquake faulting. Focal mechanisms and their spatial distributions are important for evaluating tectonic/local stress and strain fields (e.g. Townend & Zoback 2006, Terakawa & Matsu'ura 2010, Saito *et al.* 2018). To determine focal mechanisms, first-*P* or *S* polarisation inversion (e.g. Hardebeck & Shearer 2002, Thurber *et al.* 2006, Shelly *et al.* 2016) and waveform-based centroid moment tensor (CMT) inversion (e.g. Dziewonski *et al.* 1981, Kanamori & Rivera 2008, Vallée *et al.* 2011, Ekström *et al.* 2012) techniques have been widely used in the world. One-dimensional (1D) Earth models are assumed in typical focal mechanism determination methods. In regions with complex three-dimensional (3D) heterogeneous structures, first-motion solutions using the 1D Earth model systematically show mis estimations (e.g. Takemura *et al.* 2016). Although CMT methods based on long-period (> 10 s) waveforms can be applicable only for moderate-to-large earthquakes due to signal-to-noise problems for long-period components, their evaluations of source parameters are generally robust against structural heterogeneities in comparison to first-motion solutions.

Along the Nankai Trough, megathrust earthquakes have repeatedly occurred at intervals of 100–150 years (e.g. Ando 1975). Evaluating seismicity around this region is important for contributing to the understanding of megathrust earthquakes, such as evaluating stress accumulation/release processes on plate boundaries. In Japan, regular and slow earthquakes have been systematically monitored by the seismic networks of the Monitoring of Waves on Land and Seafloor (MOWLAS; https://doi.org/10.17598/NIED.0009) operated by the National Research Institute for Earth Science and Disaster Resilience (NIED; Okada *et al.* 2004). According to the combined earthquake catalogues of the International Seismological Centre-Global Earthquake Model (ISC-GEM; Storchak *et al.* 2013), the Japan Meteorological Agency (JMA), and the NIED F-net (Fukuyama *et al.* 1998, Kubo *et al.* 2002), the seismicity of regular earthquakes along the Nankai Trough, especially interplate earthquakes, is quite low. Figure 1 shows the spatial distribution of regular earthquakes with moment magnitudes (*Mw*) of 4.3–6.5 that occurred from April 2004 to August 2019, as listed in the F-net moment tensor (F-net MT) catalogue. A few shallow offshore earthquakes occurred in the Tonankai and Nankai regions and their focal mechanisms in the F-net catalogue were not characterised by low-angle thrust faulting. In other words, no earthquakes suggesting faulting on the plate boundary around the Tonankai and Nankai regions are listed in the F-net MT catalogue.

On 1 April 2016, the *Mw* 5.8 earthquake, called "2016 southeast off the Kii Peninsula earthquake", occurred in the Tonankai region (marked A in Figure 1). The F-net MT solution of this earthquake was characterised by high-angle (38°) reverse faulting below the upper surface of the Philippine Sea Plate, indicating it was an intraslab earthquake. However, a detailed analysis of this earthquake revealed that it could be modelled by a low-angle thrust faulting at a depth of approximately 10 km, suggesting seismic slip along the plate boundary (e.g. Wallace *et al.* 2016, Nakano, Hyodo, *et al.* 2018, Takemura, Kimura, *et al.* 2018). Source models suggested in these studies were also consistent with a model based on observed tsunami data (Kubota *et al.* 2018). In regions with a thick accretionary prism, characteristics of surface wave propagation are significantly affected by a low-velocity accretionary prism (e.g. Shapiro *et al.* 1998, Furumura *et al.* 2008, Nakamura *et al.* 2015, Volk *et al.* 2017, Gomberg 2018, Kaneko *et al.* 2019). Thus, the focal mechanisms of other offshore earthquakes along the Nankai Trough could be incorrectly estimated using conventional 1D regional MT inversion, even for long-period displacements. Indeed, shallow very low frequency earthquakes along the Nankai Trough have been interpreted as low-angle thrust faulting on the plate boundary by using offshore seismic observations (e.g. Sugioka *et al.* 2012, Nakano, Hori, *et al.* 2018), but their focal mechanisms based on 1D analysis of onshore observations were high-angle reverse faulting mechanisms within the accretionary prism (Ito & Obara 2006). To evaluate seismic activity along the Nankai Trough more precisely, offshore earthquakes listed in the previous 1D catalogues require re-analysis.

Parallel simulation codes of seismic wave propagation (e.g. Gokhberg & Fichtner 2016, Maeda *et al.* 2017) and 3D seismic velocity structure models (e.g. Nishida *et al.* 2008, Eberhart-Phillips *et al.* 2010, Koketsu *et al.* 2012) enable the simulation of Green's functions propagating through realistic 3D Earth models (hereafter called '3D Green's functions'), which have been used to develop CMT inversions (e.g. Ramos-Martínez & McMechan 2001, Lee *et al.* 2013, Hejrani *et al.* 2017, Okamoto *et al.* 2018, Takemura, Kimura, *et al.* 2018, Takemura, Matsuzawa, *et al.* 2018, 2019, Wang & Zhan 2019). Although the resolution of detailed source characteristics for offshore earthquakes deriving using the 3D CMT method and onshore seismograms are limited compared to those using offshore observations, these methods provide similar focal mechanisms and centroid locations. Thus, offshore seismic activity, including earthquakes before offshore seismic observations, can be effectively evaluated.

To investigate the decade-scale seismicity of offshore earthquakes along the Nankai Trough, we re-evaluated focal mechanisms based on CMT inversion using 3D Green's function datasets, which were evaluated by numerical simulations of seismic wave propagation in a regional 3D velocity structure model. Then, to investigate spatial variation in slip behaviours on the plate boundary along the Nankai Trough, we compared the spatial distribution of focal mechanisms based on the 3D CMT technique with the spatial distribution of slip-deficit rates (Noda *et al.* 2018), slow slip events (SSEs; Miyazaki *et al.* 2006, Nishimura *et al.* 2013, Kobayashi 2014, Takagi *et al.* 2016, 2019, Yokota & Ishikawa 2019), shallow low-frequency tremors (LFTs; Yamashita *et al.* 2015), shallow very low-frequency earthquakes (VLFEs; Takemura, Noda, *et al.* 2019), and the 1968 Hyuga-nada earthquake (Yagi *et al.* 1998).

2. Data and Methods

We used three-component velocity seismograms of F-net (National Research Institute for Earth Science and Disaster Resilience 2019), the sensors of which have been systematically monitored (Kimura *et al.* 2015). To conduct CMT inversion of the target earthquakes, we applied a band-pass filter with passed periods of 25–100 s to velocity seismograms. We selected a 25–100 s period band because ground motions for periods of 8–20 s are significantly affected by internal structures of the accretionary prism along the Nankai Trough (e.g. Nakamura *et al.* 2015, Guo *et al.* 2016, Takemura, Kimura, *et al.* 2018, Takemura, Kubo, *et al.* 2019). We obtained displacement waveforms by calculating time integration of each filtered velocity record. The target earthquakes occurred within the region of assumed source grids (grey crosses in Figure 2) between April 2004 and August 2019, and values of Mw in the F-net catalogue ranging from 4.3 to 6.5. According to the signal-to-noise ratios for the target period band, the magnitude range of the analysed earthquake was determined by trial and error. Source grids were uniformly distributed at horizontal intervals of 0.1°. Depths of source grids ranged from 6 to 50 km at an interval of 2 km. The total number of source grids was 61,433.

Green's functions were evaluated by solving equations of motion in the 3D viscoelastic medium model based on the finite-difference method (FDM) simulations. The 3D simulation model covered an area of 900 × 1,000 × 100 km^3, which was discretised by grid intervals of 0.5 km in the horizontal direction and 0.2 km in the vertical direction. We used a parallel simulation code of OpenSWPC (Maeda *et al.* 2017), which includes the reciprocal calculation mode for effectively evaluating Green's functions. The reciprocal calculation has proved very useful in the case that the number of seismic source grids is significantly larger than the number of seismic stations (e.g. Eisner & Clayton 2001, Petukhin *et al.* 2016, Hejrani *et al.* 2017, Okamoto *et al.* 2018). We obtained a total of approximately 35,000,000 Green's function SAC files from 61,433 source grids to 32 F-net stations (black and blue filled triangles in Figure 2) via 96 reciprocal FDM calculations. The source time function of each Green's function was the Küpper wavelet with a duration of 1 s.

The 3D velocity model of Koketsu *et al.* (2012) was used, as it has been widely applied in studies of seismic ground motions across Japan (e.g. Iwaki et al., 2018; Miyazawa, 2019; Park & Ishii, 2018; Takemura et al., 2017). The topography model in our simulations was the ETOPO1 model (Amante & Eakins 2009). The *P*- and *S*-wave velocities and density (V_P, V_S and ρ) in the seawater layer were 1.5 km/s, 0.0 km/s and 1.04 g/cm^3, respectively. The air column was modelled as a vacuum with V_P of 0.0 km/s, V_S of 0.0 km/s and ρ of 0.001 g/cm^3. The minimum V_S in the solid column of 1.5 km/s was assumed. Simulations were conducted using the computer system of the Earthquake and Volcano Information Center at the Earthquake Research Institute, the University of Tokyo. Each simulation required 385 GBytes of computer memory and a wall-clock time of 2.5 hours and was performed using parallel computing with 432 cores to evaluate seismic wave propagation of 200 s with 20,000 time-step calculations. According to our grid and model settings, our FDM simulation can precisely evaluate long-period (> 10 s) seismic wave propagation.

Examples of Green's functions are illustrated in the right panels of Figure 2. The source (red star) was located at a depth of 10 km, near the plate boundary. We employed the Cartesian coordinate system of Aki & Richards (2002), where x, y, and z are taken as north, east, and down, respectively. Due to the low-velocity accretionary prism and seawater, durations of surface waves were amplified and elongated. In particular, where M_{xy} = 1.0 (i.e. a pure strike-slip with strike angle of 0°, dip angle of 90°, and rake angle of 0°), Love waves in horizontal components were strong and long. We assumed six-element moment tensors for the CMT inversions, which includes five double couple and an isotropic moment tensors (e.g. Kikuchi & Kanamori 1991).

In the CMT inversions, we basically used Green's functions at F-net stations within epicentral distances of 100–400 km from the initial epicentre. The initial epicentre was obtained from the F-net MT catalogue. In cases where earthquake Mw < 4.5, we selected a distance range of 100–350 km due to the signal-to-noise ratio of the observed waveforms for the analysed period. We visually checked the filtered displacement waveforms and discarded noisy ones. Centroid location and time of the analysed earthquake were determined using grid search inversion (e.g. Lee et al., 2014; Takemura, Matsuzawa, et al., 2019; Tsuruoka et al., 2009). Because the analysis period range was longer than the source durations of target earthquakes with *Mw* = 4.3–6.5, we did not estimate source durations of these events. A set of Green's functions at the source grids, which were located in a ± 0.4° region from the initial epicentre and were distributed at depths of 6–50 km, was selected for the grid search inversion.

The CMT inversions were conducted for each selected source grid every 1 s from three minutes before the origin minute as recorded in the F-net catalogue. We used a 200-s time window for each CMT inversion. After CMT inversion at all of the selected source grids, to identify the optimal solution, we evaluated variance reductions (VRs) between the observed and synthetic displacement seismograms for periods of 25—100 s. The VR could then be evaluated using the following equation:

$$VR = \left[1 - \frac{\sum_{i=1}^{N_S} \int \left(u_i^{Obs.}(t) - u_i^{Syn.}(t)\right)^2 dt}{\sum_{i=1}^{N_S} \int \left(u_i^{Obs.}(t)\right)^2 dt}\right] \times 100\ [\%] \quad (1)$$

where N_S is the number of stations and $u_i^{Obs.}$ and $u_i^{Syn.}$ are the time-series of observed and synthetic displacements, respectively. If observed and synthetic seismograms are perfectly matched, VR is 100 %. The solution with the maximum VR was considered the optimal solution, providing the optimal centroid location, depth, time, focal mechanism, and seismic moment of each earthquake. In the case that the optimal solution was located at the edges of the initial assumed grid set, we performed the CMT inversion again using Green's functions for a broader source grid dataset. Our grid search CMT inversion required approximately 15–20 minutes using a typical, single-core desktop machine.

3. Results

We obtained a total of 215 CMT solutions for moderate earthquakes that occurred between April 2004 and August 2019. We discarded the solutions with a maximum VR of less than 20%. Our 3D CMT catalogue was described in Global CMT (GCMT) format and listed in the Supplementary data (Table S1). The size distribution and magnitude-time diagram of our 3D CMT catalogue are shown in Figures S1 and S2. We note that the optimal solutions at the edges of assumed all source grids may include some shifts outside the edges of the assumed source grids (Figure 2). These earthquakes (at grid edges) were concentrated around southern Kyushu and eastern edge of Izu.

Figures 3 and 4 show examples of CMT solutions for southeast off the Kii Peninsula earthquake (1 April 2016) and the Hyuga-nada earthquake (10 May 2019), respectively. In our previous study (Takemura, Kimura, *et al.* 2018), the 2016 southeast off the Kii Peninsula earthquake was also analysed. The epicentre location and origin time were fixed in the previous study. We re-analysed this earthquake via full 3D CMT inversion, which estimates centroid location, depth, time, and moment tensor. The F-net MT solution of this earthquake was a high-angle (38°) reverse faulting mechanism (grey focal sphere in Figure 3). Its optimal solution is a *Mw* 5.9 low-angle (10.1°) thrust faulting at a depth of 10 km (Figure 3), where the plate boundary closely exists (e.g. Kamei et al., 2012; Park et al., 2010). The synthetic seismograms of the optimal solution corresponded well with the observations. The depth variation of VRs illustrated a clear peak around the optimal depth. The centroid depth of this earthquake was well constrained by our CMT inversion. Takemura, Kimura, et al. (2018) numerically demonstrated that the low-velocity accretionary prism just above the seismic source—which controls long-period surface wave propagation—provides a better constraint on the centroid depth. According to the estimated focal mechanism and centroid depth, this earthquake was considered as the faulting on the plate boundary. Furthermore, the CMT result was consistent with models estimated by offshore observations (Wallace *et al.* 2016, Kubota *et al.* 2018, Nakano, Hyodo, *et al.* 2018).

Figure 4 shows the results of the CMT inversion and waveform fitting for the off the Hyuga-nada earthquake on 10 May 2019. The F-net MT solution was also a high-angle (33°) reverse faulting. The optimal CMT solution indicated a *Mw* 6.2 low-angle (15.6°) thrust faulting. The dip angle agreed well with that of the Philippine Sea Plate around this earthquake (e.g. Nakajima & Hasegawa 2007, Koketsu *et al.* 2012). The synthetic waveforms also corresponded well to observed ones. Although the optimal depth (26 km) was determined to be close to the upper surface of the Philippine Sea Plate (approximately 27 km), a high VR (> 80%) area was found within a wider depth range (16–32 km). Because the depth of this earthquake was deeper than the 2016 southeast off the Kii Peninsula earthquake, the effects of the low-velocity accretionary prism might not have been so strong. Thus, the depth resolution of the CMT solutions might not be good when compared to the case of the 2016 southeast off the Kii Peninsula earthquake. To constrain the hypocentre depth more sharply, additional data, such as shorter-period (~ 4 s) first-arrival *P*-wave waveforms, would need to be considered (e.g. Okamoto *et al.* 2018, Takemura, Kimura, *et al.* 2018, Wang & Zhan 2019).

Figure 5 shows a comparison of the estimated focal mechanisms for the F-net and our 3D

CMT catalogues. Our CMT solutions of earthquakes in onshore regions were not significantly different from the F-net ones. However, our CMT solutions differed to those based on 1D analysis. In particular, dip angles and centroid depths of offshore earthquakes—which are important for distinguishing interplate and intraslab earthquakes—were different. This was clearly illustrated in detailed comparisons of seismicity southeast off the Kii Peninsula and off the Hyuga-nada (Figures 6, 7, S3, and S4). The dip angles of offshore earthquakes that occurred outside of onshore seismic arrays were poorly estimated by the conventional 1D CMT inversion due to the lack of the subducting oceanic plate and the accretionary prism (e.g. Takemura, Kimura, *et al.* 2018, Takemura, Matsuzawa, *et al.* 2018).

We focused our attention on seismicity southeast off the Kii Peninsula and the Hyuga-nada (local names are illustrated in Figure 1), where seismic activities are relatively high in the Nankai subduction zone. Figure 6 shows spatial distributions of the CMT solutions southeast off the Kii Peninsula. We also plotted shallow VLFEs in the catalogue of Takemura, Matsuzawa, et al. (2019) as grey focal spheres. Shallow VLFEs, which were characterised by low-angle thrust faulting, were concentrated near the trench. In the region with shallow VLFE active, no CMT solution suggesting slip on the plate boundary was estimated. On the down-dip side of the shallow VLFE region, a low-angle thrust faulting mechanism was estimated at a depth near the plate boundary (along profile A in Figure 6). This earthquake is the 2016 southeast off the Kii Peninsula earthquake (Figure 3). Almost all of the other earthquakes plotted in Figure 6 are aftershocks of the 2004 *Mw* 7.5 intraslab earthquake that occurred on 5 September 2004 southeast off the Kii Peninsula. Our CMT solutions of these aftershocks were separately distributed at depths within the oceanic crust and mantle (10–15 and 20–30 km depths). This separation corresponded well to the hypocentre depth distributions of the aftershocks of the *Mw* 7.5 earthquake as determined using temporal ocean-bottom seismometers (e.g. Sakai et al., 2005). On the other hand, almost all the centroid depths of the F-net solutions were concentrated within the crust and oceanic crust (5–15 km depths; Figure S3).

Figure 7 shows the spatial distribution of the CMT solutions around the Hyuga-nada region. Our CMT solutions characterised by low-angle thrust faulting mechanisms were distributed across the region with average slip rates of approximately 20–40 mm/yr as inferred from small repeating earthquakes (Igarashi 2010, Yamashita *et al.* 2012). The optimal centroid depths of such thrust solutions were concentrated around the plate boundary (profiles B and C in Figure 7). The dip angles of the F-net MT solutions at depths around the plate boundary were slightly higher than those of the plate boundary, as shown in Figure S4. This also might have been due to a lack of 3D geometry of the subducting oceanic plate in the 1D analysis.

4. Discussion

4.1. Slip behaviours on the plate boundary along the Nankai Trough

In order to discuss slip behaviours on the plate boundary, we selected low-angle thrust faulting solutions at depths around the plate boundary from our 3D CMT catalogue. These selected events could be interpreted as seismic slips on the plate boundary. Figure 8 shows the spatial distribution of earthquakes with low-angle (< 25°) thrust faulting solutions at depths around the plate boundary along the Nankai Trough.

In Figure 8, we also plotted related seismic activity. The large coseismic slip area of the 1968 *Mw* 7.5 earthquake (Yagi *et al.* 1998) is indicated by the blue area in Figure 8. The cumulative deep SSE slips in each grid were determined by summing slips of each SSE in each catalogue (Nishimura *et al.* 2013, Takagi *et al.* 2016, 2019). We then evaluated the SSE slip rates by dividing the cumulative SSE slip at each grid by the analysis period of each catalogue. The SSE slip rate indicates the activity of deep, slow earthquakes (e.g. Ito *et al.* 2007, Obara & Kato 2016). We did not calculate SSE slip rates forof shallow SSEs reported by Yokota & Ishikawa (2019) because the number of detected events was still few at each region. For similar reasons, the long-term SSEs off the Kii Channel (Kobayashi 2014) and Tokai (Miyazaki *et al.* 2006) regions were also excluded from the SSE slip rate calculation. Thus, we plotted the fault configurations or large slip areas of long-term SSEs and shallow SSEs. We also plotted shallow LFTs (Yamashita *et al.* 2015) and shallow VLFEs (Takemura, Noda, *et al.* 2019) as indicators of shallow, slow earthquake activity. The spatial distribution of slip-deficit rates from GNSS and GNSS-A observations by Noda et al. (2018), is plotted using blue contour lines in Figure 8.

At deeper depths (30–40 km), deep slow earthquakes were active, especially in areas with high SSE slip rates, but no interplate regular earthquakes were found. Although SSEs were not removed in the slip-deficit rate estimation of Noda et al. (2018)—except for long-term SSEs at the Bungo Channel—the regions with deep SSEs were characterised by low (20–40 mm/y) slip-deficit rates. At shallower depths (< 30 km) in the offshore region, regular earthquakes, slow earthquakes, and high (> 60 mm/y) slip-deficit zones were separately distributed. Similar separation of the repeating earthquakes, slow earthquakes, and large coseismic slip areas of megathrust earthquakes at shallower depths were observed in the regions of Tohoku (e.g. Matsuzawa *et al.* 2015, Nishikawa *et al.* 2019, Tanaka *et al.* 2019), Central Ecuador (e.g. Rolandone *et al.* 2018, Vaca *et al.* 2018) and Costa Rica (e.g. Dixon *et al.* 2014). In particular, Nishikawa et al. (2019) pointed out that slow earthquakes were complementarily distributed in the regions surrounding the large coseismic slip area of the 2011 *Mw* 9.0 Tohoku earthquake. Takemura, Noda, et al. (2019) pointed out that shallow, slow earthquakes cluster or migrate due to the existence of pore fluid in the transitional regions between high-strength and low-strength zones of the plate boundary. According to these previous studies and our observations, we suggest that the observed separation between slip behaviours on the plate boundary along the Nankai Trough are related to the heterogeneous distribution of effective strengths on the plate boundary, which is controlled by the frictional coefficient, pore fluid pressure, and normal stress.

4.2. Regional 3D CMT inversions for the Mw 7.2 and 7.5 earthquakes southeast off the Kii Peninsula

We conducted 3D CMT inversions of offshore earthquakes with *Mw* of 4.3–6.5. During the analysis period (April 2004 to August 2019), *Mw* 7.2 and 7.5 intraslab earthquakes occurred southeast off the Kii Peninsula on 5 September 2004. Because typical *Mw* 7 class earthquakes have rupture durations of 30–50 s and fault areas of 1000–5000 km^2 (e.g. Kanamori & Brodsky 2004, Vallée & Douet 2016), precise source parameter estimation for such earthquakes is difficult based on our assumptions of the CMT inversion. We, therefore, tested the CMT inversion of the *Mw* 7.2 and 7.5 southeast off the Kii Peninsula earthquakes. Because amplitude saturation of F-net broadband seismometers occurs for regional large earthquakes, we used F-net strong motion seismometers, which have a large clip level and a similar frequency response to STS-2 seismometers. We selected F-net stations with distances of 200–500 km from the initial epicentre, which were slightly far from the original CMT settings (100–400 km).

Figures 9 and 10 show the results of CMT inversions for the *Mw* 7.2 and 7.5 earthquakes southeast off the Kii Peninsula, respectively. Detailed estimated parameters are also listed in Table S2. Signal-to-noise ratios were enough high compared to smaller (*Mw* < 4.5) earthquakes in this study but the VRs were low compared to those of moderate earthquakes. The synthetic waveforms roughly corresponded to the observed ones (Figures 9b and 10b). Due to the assumptions of a point source and simple-source time function, detailed characteristics of the observed waveforms were not successfully reproduced. Furthermore, the high (> 66%) VR areas were wider than the CMT results for moderate earthquakes within the same region (Figure 3). This suggests the likely complexity of the rupture processes and the source extents for the *Mw* 7.2 and 7.5 earthquakes. Estimated moment magnitudes were slightly smaller than those of the GCMT catalogue as a result of analysed period and the deeper centroid depths.

We also compared our CMT result for the *Mw* 7.2 earthquake with the finite-fault model (Okuwaki & Yagi 2018) conducted using teleseismic records based on Yagi & Fukahata (2011). Our horizontal centroid location was very close to an area with a large (> 3 m) coseismic slip (Figure 11). The depths of such large coseismic slips in the finite fault model ranged from 9 to 18 km but the optimal centroid depth of the 3D CMT inversion was 26 km. The finite fault model of Okuwaki & Yagi (2018) was conducted using teleseismic records and the 1D Earth model. Although this approach provides robust solutions in earthquake faulting models, depth resolutions are generally limited compared to regional analysis (e.g. see Figure 4 in Koketsu *et al.* 2011). According to the hypocentre determinations derived using ocean-bottom seismometers (Sakai *et al.* 2005, Nakano *et al.* 2015), the hypocentres of aftershocks due to the *Mw* 7.5 earthquake were distributed at depths of approximately 10–30 km. Based on this and the fault dimensions of the *Mw* 7.2 earthquake, we considered that the extension of seismic slips at depths of approximately 26 km might be possible.

5. Conclusion

We conducted 3D CMT inversions of moderate earthquakes along the Nankai Trough using the regional 3D Green's function dataset. By introducing 3D heterogeneities, our CMT method based on onshore seismograms provided better constrained focal mechanisms and centroid depths compared to regional 1D analysis of the F-net MT catalogue. Although no suggestive interplate earthquakes are listed in the 1D catalogue, some low-angle thrust faulting solutions at depths around the plate boundary were confirmed by our 3D CMT catalogue. By using our 3D CMT catalogue and previously published slow earthquake models, we illustrated the spatial distribution of slip behaviours on the plate boundary along the Nankai Trough. Regular interplate earthquakes and slow earthquakes were separately distributed on the plate boundary. These separated distributions might reflect the heterogeneous distribution of effective strength on the plate boundary. The gap zones of both regular interplate and slow earthquakes were found in the Nankai, Tonankai, and Tokai regions. These were the regions with large (> 60 mm/y) slip-deficit rates, where the plate boundary can be strongly coupled.

The regional CMT inversion of earthquakes with *Mw* > 7 was generally difficult due to their fault size and the amplitude saturation of the broadband sensors. CMT inversions for the 2004 *Mw* 7.2 and 7.5 intraslab earthquakes southeast of the Kii Peninsula were performed using the regional broadband strong motion sensors of F-net. Although signal-to-noise ratios of the observed displacements were enough good, the waveform fittings of the *Mw* 7.2 and 7.5 intraslab earthquakes were not good compared to those of typical moderate earthquakes due to fault sizes and the rupture complexity. However, the estimated focal mechanisms were very similar to those in the GCMT catalogue. Our grid search CMT inversion required approximately 15–20 minutes to run using a single-core desktop computer. This offers potential advantages for CMT-based tsunami warning systems (e.g. Reymond *et al.* 2012, Miyoshi *et al.* 2015, Inazu *et al.* 2016).

The detailed rupture processes of the *Mw* 7.2 and 7.5 earthquakes remain unclear. The regional seismic data and 3D Green's functions may provide additional constraints for large offshore earthquakes. The finite fault modelling based on the 3D Green's functions is an important but challenging issue that requires particular attention in future studies.

Acknowledgements

F-net waveform data and the F-net MT catalogue are available via the website of the National Research Institute for Earth Science and Disaster Resilience (https://doi.org/10.17598/NIED.0005). Bathymetric depth data was obtained from ETOPO1 (Amante & Eakins 2009). OpenSWPC software (Maeda *et al.* 2017) and the 3D model of Koketsu et al. (2012) were obtained from https://github.com/takuto-maeda/OpenSWPC and https://www.jishin.go.jp/evaluation/seismic_hazard_map/lpshm/12_choshuki_dat/, respectively. Generic Mapping Tools (Wessel *et al.* 2013) and Seismic Analysis Code (SAC; Helffrich *et al.* 2013) were used to make the figures and when conducting the signal processing work, respectively. The catalogue of slow earthquakes (Nishimura *et al.* 2013, Yamashita *et al.* 2015, Takagi *et al.* 2016) was downloaded from the Slow Earthquake Database website (Kano *et al.* 2018; http://www-solid.eps.s.u-tokyo.ac.jp/~sloweq/). Our CMT catalogue and CMT results of assumed source grids for each earthquake are available from https://doi.org/10.5281/zenodo.3523583. The FDM simulations of seismic wave propagation were conducted on the computer system of the Earthquake and Volcano Information Center at the Earthquake Research Institute, the University of Tokyo. This study was supported by the Japan Society for the Promotion of Science (JSPS) KAKENHI Grant Numbers 17K14382 under the Grant-in-Aid for Young Scientists (B) and 19H04626 in Scientific Research under Innovative Areas 'Science of Slow Earthquakes'.

References

Aki, K. & Richards, P. (2002) *Quantitative Seismology*, 2nd ed., University Science Books. Retrieved from https://www.ldeo.columbia.edu/~richards/Aki_Richards.html

Amante, C. & Eakins, B.W. (2009) ETOPO1 1 arc-munite global relief model: Precedures, data sources and analysis. NOAA Technical Memorandum NESDIS NGDC-24. *NOAA Tech. Memo. NESDIS NGDC-24. Natl. Geophys. Data Center, NOAA*, 19. doi:10.7289/V5C8276M

Ando, M. (1975) Source mechanisms and tectonic significance of historical earthquakes along the Nankai trough, Japan. *Tectonophysics*, **27**, 119–140. doi:10.1016/0040-1951(75)90102-X

Dixon, T.H., Jiang, Y., Malservisi, R., McCaffrey, R., Voss, N., Protti, M. & Gonzalez, V. (2014) Earthquake and tsunami forecasts: Relation of slow slip events to subsequent earthquake rupture. *Proc. Natl. Acad. Sci.*, **111**, 17039–17044. doi:10.1073/pnas.1412299111

Dziewonski, A.M., Chou, T.-A. & Woodhouse, J.H. (1981) Determination of earthquake source parameters from waveform data for studies of global and regional seismicity. *J. Geophys. Res. Solid Earth*, **86**, 2825–2852. doi:10.1029/JB086iB04p02825

Eberhart-Phillips, D., Reyners, M., Bannister, S., Chadwick, M. & Ellis, S. (2010) Establishing a versatile 3-D seismic velocity model for New Zealand. *Seismol. Res. Lett.*, **81**, 992–1000. doi:10.1785/gssrl.81.6.992

Eisner, L. & Clayton, R.W. (2001) A reciprocity method for multiple-source simulations. *Bull. Seismol. Soc. Am.*, **91**, 553–560. doi:10.1785/0120000222

Ekström, G., Nettles, M. & Dziewoński, A.M. (2012) The global CMT project 2004-2010: Centroid-moment tensors for 13,017 earthquakes. *Phys. Earth Planet. Inter.*, **200–201**, 1–9. doi:10.1016/j.pepi.2012.04.002

Fukuyama, E., Ishida, M., Dreger, D.S. & Kawai, H. (1998) Automated seismic moment tensor determination by using on-line broadband seismic waveforms. *Zisin*, **51**, 149–156. doi:10.4294/zisin1948.51.1_149

Furumura, T., Hayakawa, T., Nakamura, M., Koketsu, K. & Baba, T. (2008) Development of long-period ground motions from the Nankai trough, Japan, earthquakes: Observations and computer simulation of the 1944 Tonankai (Mw 8.1) and the 2004 SE Off-Kii Peninsula (Mw 7.4) earthquakes. *Pure Appl. Geophys.*, **165**, 585–607. doi:10.1007/s00024-008-0318-8

Gokhberg, A. & Fichtner, A. (2016) Full-waveform inversion on heterogeneous HPC systems. *Comput. Geosci.*, **89**, 260–268, Elsevier. doi:10.1016/j.cageo.2015.12.013

Gomberg, J. (2018) Cascadia Onshore-Offshore Site Response, Submarine Sediment Mobilization, and Earthquake Recurrence. *J. Geophys. Res. Solid Earth*. doi:10.1002/2017JB014985

Guo, Y., Koketsu, K. & Miyake, H. (2016) Propagation mechanism of long-period ground motions for offshore earthquakes along the nankai trough: Effects of the accretionary wedge. *Bull. Seismol. Soc. Am.*, **106**, 1176–1197. doi:10.1785/0120150315

Hardebeck, J.L. & Shearer, P.M. (2002) A new method for determining first-motion focal mechanisms. *Bull. Seismol. Soc. Am.*, **92**, 2264–2276. doi:10.1785/0120010200

Hejrani, B., Tkalčić, H. & Fichtner, A. (2017) Centroid moment tensor catalogue using a 3-D continental scale Earth model: Application to earthquakes in Papua New Guinea and the Solomon Islands. *J. Geophys. Res. Solid Earth*, **122**, 5517–5543. doi:10.1002/2017JB014230

Helffrich, G., Wookey, J. & Bastow, I. (2013) *The Seismic Analysis Code*, Cambridge: Cambridge University Press. doi:10.1017/CBO9781139547260

Igarashi, T. (2010) Spatial changes of inter-plate coupling inferred from sequences of small repeating earthquakes in Japan. *Geophys. Res. Lett.*, **37**, 1–5. doi:10.1029/2010GL044609

Inazu, D., Pulido, N., Fukuyama, E., Saito, T., Senda, J. & Kumagai, H. (2016) Near-field tsunami forecast system based on near real-time seismic moment tensor estimation in the regions of Indonesia, the Philippines, and Chile 4. Seismology. *Earth, Planets Sp.*, **68**, Springer Berlin Heidelberg. doi:10.1186/s40623-016-0445-x

Ito, Y. & Obara, K. (2006) Dynamic deformation of the accretionary prism excites very low frequency earthquakes. *Geophys. Res. Lett.*, **33**, L02311. doi:10.1029/2005GL025270

Ito, Y., Obara, K., Shiomi, K., Sekine, S. & Hirose, H. (2007) Slow earthquakes coincident with episodic tremors and slow slip events. *Science (80-.).*, **315**, 503–506. doi:10.1126/science.1134454

Iwaki, A., Maeda, T., Morikawa, N., Takemura, S. & Fujiwara, H. (2018) Effects of random 3D upper crustal heterogeneity on long-period (≥ 1 s) ground-motion simulations. *Earth, Planets Sp.*, **70**, 156. doi:10.1186/s40623-018-0930-5

Kamei, R., Pratt, R.G. & Tsuji, T. (2012) Waveform tomography imaging of a megasplay fault system in the seismogenic Nankai subduction zone. *Earth Planet. Sci. Lett.*, **317–318**, 343–353, Elsevier B.V. doi:10.1016/j.epsl.2011.10.042

Kanamori, H. & Brodsky, E.E. (2004) The physics of earthquakes. *Reports Prog. Phys.*, **67**, 1429–1496. doi:10.1088/0034-4885/67/8/R03

Kanamori, H. & Rivera, L. (2008) Source inversion of W phase: Speeding up seismic tsunami warning. *Geophys. J. Int.*, **175**, 222–238. doi:10.1111/j.1365-246X.2008.03887.x

Kaneko, Y., Ito, Y., Chow, B., Wallace, L.M., Grapenthin, R., Anastasio, E.D. & Henrys, S. (2019) Ultra-long duration of seismic ground motion arising from a thick , low velocity sedimentary wedge. *J. Geophys. Res. Solid Earth*, **124**. doi:10.1029/2019JB017795

Kano, M., Aso, N., Matsuzawa, T., Ide, S., Annoura, S., Arai, R., Baba, S., *et al.* (2018) Development of a Slow Earthquake Database, **89**, 1566–1575. doi:10.1785/0220180021

Kikuchi, M. & Kanamori, H. (1991) Inversion of complex body waves-III. *Bull. Seism. Soc. Am.*, **81**, 2335–2350. Retrieved from https://pubs.geoscienceworld.org/ssa/bssa/article/81/6/2335/102472/inversion-of-complex-body-waves-iii

Kimura, T., Murakami, H. & Matsumoto, T. (2015) Systematic monitoring of instrumentation health in high-density broadband seismic networks. *Earth, Planets Sp.*, **67**, ??? doi:10.1186/s40623-015-0226-y

Kobayashi, A. (2014) A long-term slow slip event from 1996 to 1997 in the Kii Channel, Japan. *Earth, Planets Sp.*, **66**, 1–7. doi:10.1186/1880-5981-66-9

Koketsu, K., Miyake, H. & Suzuki, H. (2012) Japan Integrated Velocity Structure Model Version 1. *Proc. 15th World Conf. Earthq. Eng.*, 1–4. Retrieved from http://www.iitk.ac.in/nicee/wcee/article/WCEE2012_1773.pdf

Koketsu, K., Yokota, Y., Nishimura, N., Yagi, Y., Miyazaki, S., Satake, K., Fujii, Y., *et al.* (2011) A unified source model for the 2011 Tohoku earthquake. *Earth Planet. Sci. Lett.*, **310**, 480–487. doi:10.1016/j.epsl.2011.09.009

Kubo, A., Fukuyama, E., Kawai, H. & Nonomura, K. (2002) NIED seismic moment tensor catalogue for regional earthquakes around Japan: Quality test and application. *Tectonophysics*, **356**, 23–48. doi:10.1016/S0040-1951(02)00375-X

Kubota, T., Suzuki, W., Nakamura, T., Chikasada, N.Y., Aoi, S., Takahashi, N. & Hino, R. (2018) Tsunami source inversion using time-derivative waveform of offshore pressure records to reduce effects of non-tsunami components. *Geophys. J. Int.*, **215**, 1200–1214, Oxford University Press. doi:10.1093/GJI/GGY345

Lee, S.-J., Liang, W.T., Cheng, H.W., Tu, F.S., Ma, K.F., Tsuruoka, H., Kawakatsu, H., *et al.* (2013) Towards real-time regional earthquake simulation I: Real-time moment tensor monitoring (RMT) for regional events in Taiwan. *Geophys. J. Int.*, **196**, 432–446. doi:10.1093/gji/ggt371

Lee, S.-J., Liu, Q., Tromp, J., Komatitsch, D., Liang, W.T. & Huang, B.S. (2014) Toward real-time regional earthquake simulation II: Real-time Online earthquake Simulation (ROS) of Taiwan earthquakes. *J. Asian Earth Sci.*, **87**, 56–68, Elsevier Ltd. doi:10.1016/j.jseaes.2014.02.009

Maeda, T., Takemura, S. & Furumura, T. (2017) OpenSWPC: an open-source integrated parallel simulation code for modeling seismic wave propagation in 3D heterogeneous viscoelastic media. *Earth, Planets Sp.*, **69**, 102, Springer Berlin Heidelberg. doi:10.1186/s40623-017-0687-2

Matsuzawa, T., Asano, Y. & Obara, K. (2015) Very low frequency earthquakes off the Pacific coast of Tohoku, Japan. *Geophys. Res. Lett.*, **42**, 4318–4325. doi:10.1002/2015GL063959

Miyazaki, S., Segall, P., McGuire, J.J., Kato, T. & Hatanaka, Y. (2006) Spatial and temporal evolution of stress and slip rate during the 2000 Tokai slow earthquake. *J. Geophys. Res. Solid Earth*, **111**, 1–17. doi:10.1029/2004JB003426

Miyazawa, M. (2019) Bayesian approach for detecting dynamically triggered very low-frequency earthquakes in the Nankai subduction zone and application to the 2016 M w 5.9 off-Kii Peninsula earthquake, Japan. *Geophys. J. Int.*, **217**, 1123–1140, Oxford University Press. doi:10.1093/gji/ggz073

Miyoshi, T., Saito, T., Inazu, D. & Tanaka, S. (2015) Tsunami modeling from the seismic CMT solution considering the dispersive effect: A case of the 2013 Santa Cruz Islands tsunami 4. Seismology. *Earth, Planets Sp.*, **67**. doi:10.1186/s40623-014-0179-6

Nakajima, J. & Hasegawa, A. (2007) Subduction of the Philippine Sea plate beneath southwestern Japan: Slab geometry and its relationship to arc magmatism. *J. Geophys. Res. Solid Earth*, **112**, 1–18. doi:10.1029/2006JB004770

Nakamura, T., Takenaka, H., Okamoto, T., Ohori, M. & Tsuboi, S. (2015) Long-period ocean-bottom motions in the source areas of large subduction earthquakes. *Sci. Rep.*, **5**, 1–2. doi:10.1038/srep16648

Nakano, M., Hori, T., Araki, E., Kodaira, S. & Ide, S. (2018) Shallow very-low-frequency earthquakes accompany slow slip events in the Nankai subduction zone. *Nat. Commun.*, **9**, 984. doi:10.1038/s41467-018-03431-5

Nakano, M., Hyodo, M., Nakanishi, A., Yamashita, M., Hori, T., Kamiya, S. ichiro, Suzuki, K., *et al.* (2018) The 2016 Mw5.9 earthquake off the southeastern coast of Mie Prefecture as an indicator of preparatory processes of the next Nankai Trough megathrust earthquake. *Prog. Earth Planet. Sci.*, **5**, Progress in Earth and Planetary Science. doi:10.1186/s40645-018-0188-3

Nakano, M., Nakamura, T. & Kaneda, Y. (2015) Hypocenters in the nankai trough determined by using data from both ocean-bottom and land seismic networks and a 3D velocity structure model: Implications for seismotectonic activity. *Bull. Seismol. Soc. Am.*, **105**, 1594–1605. doi:10.1785/0120140309

National Research Institute for Earth Science and Disaster Resilience. (2019) NIED F-net. *Natl. Res. Inst. Earth Sci. Disaster Resil.*, National Research Institute for Earth Science and Disaster Resilience. doi:10.17598/NIED.0005

Nishida, K., Kawakatsu, H. & Obara, K. (2008) Three-dimensional crustal S wave velocity structure in Japan using microseismic data recorded by Hi-net tiltmeters. *J. Geophys. Res. Solid Earth*, **113**, 1–22. doi:10.1029/2007JB005395

Nishikawa, T., Matsuzawa, T., Ohta, K., Uchida, N., Nishimura, T. & Ide, S. (2019) The slow earthquake spectrum in the Japan Trench illuminated by the S-net seafloor observatories. *Science (80-.).*, **365**, 808–813. doi:10.1126/science.aax5618

Nishimura, T., Matsuzawa, T. & Obara, K. (2013) Detection of short-term slow slip events along the Nankai Trough, southwest Japan, using GNSS data. *J. Geophys. Res. Solid*

Earth, **118**, 3112–3125, Wiley-Blackwell. doi:10.1002/jgrb.50222

Noda, A., Saito, T. & Fukuyama, E. (2018) Slip-deficit rate distribution along the Nankai trough, southwest Japan, with elastic lithosphere and viscoelastic asthenosphere. *J. Geophys. Res. Solid Earth*, **123**, 8125–8142. doi:10.1029/2018JB015515

Obara, K. & Kato, A. (2016) Connecting slow earthquakes to huge earthquakes. *Science (80-.).*, **353**, 253–257. doi:10.1126/science.aaf1512

Okada, Y., Kasahara, K., Hori, S., Obara, K., Sekiguchi, S., Fujiwara, H. & Yamamoto, A. (2004) Recent progress of seismic observation networks in Japan —Hi-net, F-net, K-NET and KiK-net—. *Earth, Planets Sp.*, **56**, xv–xxviii. doi:10.1186/BF03353076

Okamoto, T., Takenaka, H. & Nakamura, T. (2018) Evaluation of accuracy of synthetic waveforms for subduction-zone earthquakes by using a land–ocean unified 3D structure model. *Earth, Planets Sp.*, **70**, Springer Berlin Heidelberg. doi:10.1186/s40623-018-0871-z

Okuwaki, R. & Yagi, Y. (2018) Seismic source model for the Mw 7.2 2004 Kii peninsula, Japan, earthquake. *Github*. doi:10.5281/zenodo.1493833

Park, J.-O., Fujie, G., Wijerathne, L., Hori, T., Kodaira, S., Fukao, Y., Moore, G.F., *et al.* (2010) A low-velocity zone with weak reflectivity along the Nankai subduction zone. *Geology*, **38**, 283–286. doi:10.1130/G30205.1

Park, S. & Ishii, M. (2018) Near-surface compressional and shear wave speeds constrained by body-wave polarization analysis. *Geophys. J. Int.*, **213**, 1559–1571. doi:10.1093/gji/ggy072

Petukhin, A., Miyakoshi, K., Tsurugi, M., Kawase, H. & Kamae, K. (2016) Visualization of Green's function anomalies for megathrust source in Nankai Trough by reciprocity method. *Earth, Planets Sp.*, **68**, Earth, Planets and Space. doi:10.1186/s40623-016-0385-5

Ramos-Martínez, J. & McMechan, G.A. (2001) Source-parameter estimation by full waveform inversion in 3D heterogeneous, viscoelastic, anisotropic media. *Bull. Seismol. Soc. Am.*, **91**, 276–291. doi:10.1785/0120000017

Reymond, D., Okal, E.A., Hébert, H. & Bourdet, M. (2012) Rapid forecast of tsunami wave heights from a database of pre-computed simulations, and application during the 2011 Tohoku tsunami in French Polynesia. *Geophys. Res. Lett.*, **39**, 1–6. doi:10.1029/2012GL051640

Rolandone, F., Nocquet, J.M., Mothes, P.A., Jarrin, P., Vallée, M., Cubas, N., Hernandez, S., *et al.* (2018) Areas prone to slow slip events impede earthquake rupture propagation and promote afterslip. *Sci. Adv.*, **4**, 2–10. doi:10.1126/sciadv.aao6596

Saito, T., Noda, A., Yoshida, K. & Tanaka, S. (2018) Shear strain energy change caused by the interplate coupling along the Nankai Trough: An integration analysis using stress tensor inversion and slip deficit inversion. *J. Geophys. Res. Solid Earth*.

doi:10.1029/2018JB015839

Sakai, S., Yamada, T., Shinohara, M., Hagiwara, H., Kanazawa, T., Obana, K., Kodaira, S., *et al.* (2005) Urgent aftershock observation of the 2004 off the Kii Peninsula earthquake using ocean bottom seismometers. *Earth Planets Sp.*, **57**, 363–368. doi:10.1186/BF03352577

Shapiro, N.M., Campillo, M., Singh, S.K. & Pacheco, J. (1998) Seismic channel waves in the accretionary prism of the Middle America Trench. *Geophys. Res. Lett.*, **25**, 101–104. doi:10.1029/97GL03492

Shelly, D.R., Hardebeck, J.L., Ellsworth, W.L. & Hill, D.P. (2016) A new strategy for earthquake focal mechanisms using waveform-correlation-derived relative polarities and cluster analysis: Application to the 2014 Long Valley Caldera earthquake swarm. *J. Geophys. Res. Solid Earth*, **121**, 8622–8641. doi:10.1002/2016JB013437

Storchak, D.A., Giacomo, D. Di, Bondár, I., Engdahl, E.R., Harris, J., Lee, W.H.K. & Villaseñor, A. (2013) Public Release of the ISC – GEM Global Instrumental Earthquake Catalogue (1900 – 2009). doi:10.1785/0220130034

Sugioka, H., Okamoto, T., Nakamura, T., Ishihara, Y., Ito, A., Obana, K., Kinoshita, M., *et al.* (2012) Tsunamigenic potential of the shallow subduction plate boundary inferred from slow seismic slip. *Nat. Geosci.*, **5**, 414–418, Nature Publishing Group. doi:10.1038/ngeo1466

Takagi, R., Obara, K. & Maeda, T. (2016) Slow slip event within a gap between tremor and locked zones in the Nankai subduction zone. *Geophys. Res. Lett.*, **43**, 1066–1074. doi:10.1002/2015GL066987

Takagi, R., Uchida, N. & Obara, K. (2019) Along-Strike Variation and Migration of Long-Term Slow Slip Events in the Western Nankai Subduction Zone, Japan. *J. Geophys. Res. Solid Earth*, **124**, 3853–3880. doi:10.1029/2018JB016738

Takemura, S., Kimura, T., Saito, T., Kubo, H. & Shiomi, K. (2018) Moment tensor inversion of the 2016 southeast offshore Mie earthquake in the Tonankai region using a three-dimensional velocity structure model: effects of the accretionary prism and subducting oceanic plate. *Earth, Planets Sp.*, **70**, 50, Springer Berlin Heidelberg. doi:10.1186/s40623-018-0819-3

Takemura, S., Kobayashi, M. & Yoshimoto, K. (2017) High-frequency seismic wave propagation within the heterogeneous crust: Effects of seismic scattering and intrinsic attenuation on ground motion modelling. *Geophys. J. Int.*, **210**, 1806–1822. doi:10.1093/gji/ggx269

Takemura, S., Kubo, H., Tonegawa, T., Saito, T. & Shiomi, K. (2019) Modeling of Long-Period Ground Motions in the Nankai Subduction Zone: Model Simulation Using the Accretionary Prism Derived from Oceanfloor Local S-Wave Velocity Structures. *Pure Appl. Geophys.*, **176**, 627–647, Birkhauser Verlag AG. doi:10.1007/s00024-018-2013-8

Takemura, S., Matsuzawa, T., Kimura, T., Tonegawa, T. & Shiomi, K. (2018) Centroid Moment Tensor Inversion of Shallow Very Low Frequency Earthquakes Off the Kii Peninsula, Japan, Using a Three-Dimensional Velocity Structure Model. *Geophys. Res. Lett.*, **45**, 6450–6458, Wiley-Blackwell. doi:10.1029/2018GL078455

Takemura, S., Matsuzawa, T., Noda, A., Tonegawa, T., Asano, Y., Kimura, T. & Shiomi, K. (2019) Structural Characteristics of the Nankai Trough Shallow Plate Boundary Inferred From Shallow Very Low Frequency Earthquakes. *Geophys. Res. Lett.*, **46**, 4192–4201, Blackwell Publishing Ltd. doi:10.1029/2019GL082448

Takemura, S., Noda, A., Kubota, T., Asano, Y., Matsuzawa, T. & Shiomi, K. (2019) Migrations and Clusters of Shallow Very Low Frequency Earthquakes in the Regions Surrounding Shear Stress Accumulation Peaks along the Nankai Trough. *Geophys. Res. Lett.*, 2019GL084666. doi:10.1029/2019GL084666

Takemura, S., Shiomi, K., Kimura, T. & Saito, T. (2016) Systematic difference between first - motion and waveform - inversion solutions for shallow offshore earthquakes due to a low - angle dipping slab. *Earth, Planets Sp.*, 1–8, Springer Berlin Heidelberg. doi:10.1186/s40623-016-0527-9

Tanaka, S., Matsuzawa, T. & Asano, Y. (2019) Shallow Low-Frequency Tremor in the Northern Japan Trench Subduction Zone. *Geophys. Res. Lett.*, **46**, 5217–5224. doi:10.1029/2019GL082817

Terakawa, T. & Matsu'ura, M. (2010) The 3-D tectonic stress fields in and around Japan inverted from centroid moment tensor data of seismic events. *Tectonics*, **29**, 1–14. doi:10.1029/2009TC002626

Thurber, C., Zhang, H., Waldhauser, F., Hardebeck, J., Michael, A. & Eberhart-Phillips, D. (2006) Three-dimensional compressional wavespeed model, earthquake relocations, and focal mechanisms for the Parkfield, California, region. *Bull. Seismol. Soc. Am.*, **96**, 38–49. doi:10.1785/0120050825

Townend, J. & Zoback, M.D. (2006) Stress, strain, and mountain building in central Japan. *J. Geophys. Res. Solid Earth*, **111**, 1–11. doi:10.1029/2005JB003759

Tsuruoka, H., Kawakatsu, H. & Urabe, T. (2009) GRiD MT (grid-based real-time determination of moment tensors) monitoring the long-period seismic wavefield. *Phys. Earth Planet. Inter.*, **175**, 8–16. doi:10.1016/j.pepi.2008.02.014

Vaca, S., Vallée, M., Nocquet, J.M., Battaglia, J. & Régnier, M. (2018) Recurrent slow slip events as a barrier to the northward rupture propagation of the 2016 Pedernales earthquake (Central Ecuador). *Tectonophysics*, **724–725**, 80–92, Elsevier. doi:10.1016/j.tecto.2017.12.012

Vallée, M., Charléty, J., Ferreira, A.M.G., Delouis, B. & Vergoz, J. (2011) SCARDEC: A new technique for the rapid determination of seismic moment magnitude, focal mechanism and source time functions for large earthquakes using body-wave deconvolution. *Geophys. J. Int.*, **184**, 338–358. doi:10.1111/j.1365-246X.2010.04836.x

Vallée, M. & Douet, V. (2016) A new database of source time functions (STFs) extracted from the SCARDEC method, **257**, 149–157. doi:10.1016/j.pepi.2016.05.012

Volk, O., Shani-kadmiel, S., Gvirtzman, Z. & Tsesarsky, M. (2017) 3D Effects of Sedimentary Wedges and Subsurface Canyons : Ground-Motion Amplification in the Israeli Coastal Plain, **107**. doi:10.1785/0120160349

Wallace, L.M., Araki, E., Saffer, D., Wang, X., Roesner, A., Kopf, A., Nakanishi, A., *et al.* (2016) Near-field observations of an offshore M w 6.0 earthquake from an integrated seafloor and subseafloor monitoring network at the Nankai Trough, southwest Japan. *J. Geophys. Res. Solid Earth*, **121**, 8338–8351. doi:10.1002/2016JB013417

Wang, X. & Zhan, Z. (2019) Moving from 1D to 3D velocity model : automated waveform-based earthquake moment tensor inversion in the Los Angeles region. *Geophys. J. Int.* doi:10.1093/gji/ggz435

Wessel, P., Smith, W.H.F., Scharroo, R., Luis, J. & Wobbe, F. (2013) Generic mapping tools: Improved version released. *Eos (Washington. DC).*, **94**, 409–410. doi:10.1002/2013EO450001

Yagi, Y. & Fukahata, Y. (2011) Introduction of uncertainty of Green's function into waveform inversion for seismic source processes. *Geophys. J. Int.*, **186**, 711–720. doi:10.1111/j.1365-246X.2011.05043.x

Yagi, Y., Kikuchi, M., Yoshida, S. & Yamanaka, Y. (1998) Source Process of the Hyuga-nada Earthquake of April 1, 1968 (MJMA 7.5), and its Relationship to the Subsequent Seismicity. *Zisin (Journal Seismol. Soc. Japan. 2nd ser.)*, **51**, 139–148. doi:10.4294/zisin1948.51.1_139

Yamashita, Y., Shimizu, H. & Goto, K. (2012) Small repeating earthquake activity, interplate quasi-static slip, and interplate coupling in the Hyuga-nada, southwestern Japan subduction zone. *Geophys. Res. Lett.*, **39**, 1–5. doi:10.1029/2012GL051476

Yamashita, Y., Yakiwara, H., Asano, Y., Shimizu, H., Uchida, K., Hirano, S., Umakoshi, K., *et al.* (2015) Migrating tremor off southern Kyushu as evidence for slow slip of a shallow subduction interface. *Science (80-.).*, **348**, 676–679. doi:10.1126/science.aaa4242

Yokota, Y. & Ishikawa. (2019) Shallow long-term slow slip events along the Nankai Trough detected by the GNSS-A. *EarthArXiv*. doi:10.31223/osf.io/vq6ca

Figures

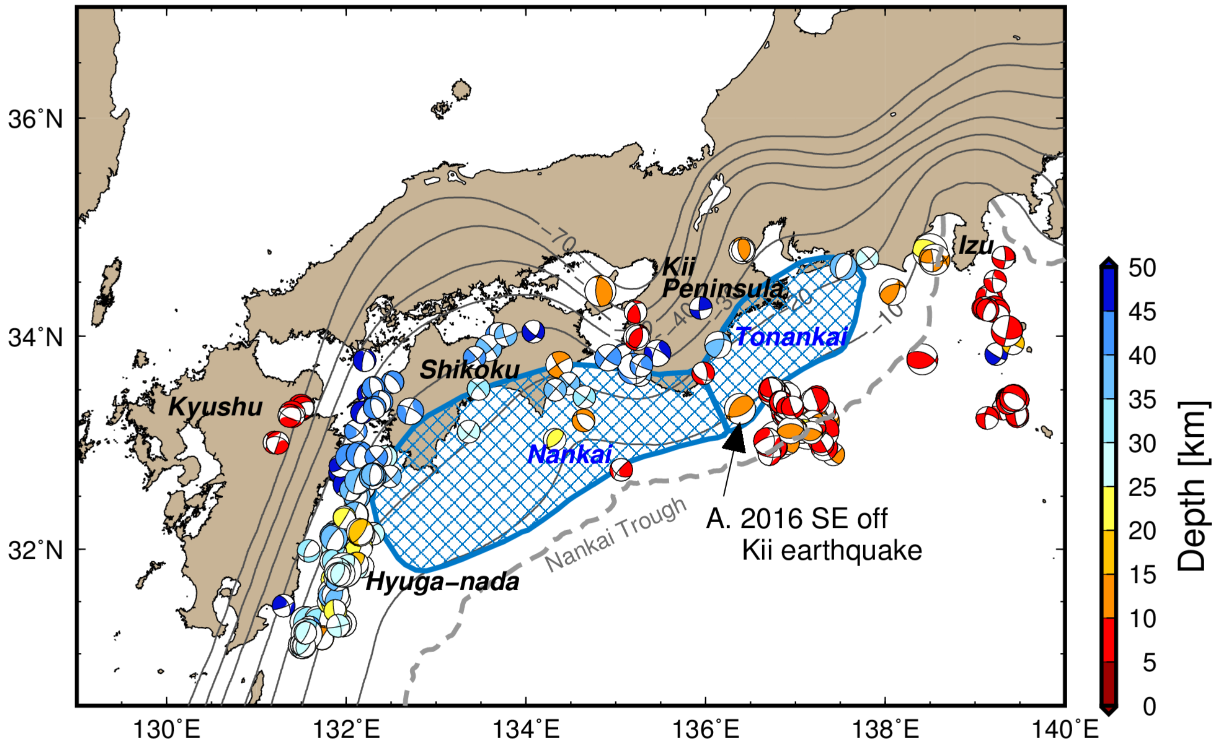

Figure 1. Map of the study region. The black contour lines are the iso-depth contour lines of the upper surface of the Philippine Sea Plate of Koketsu *et al.* (2012). Focal mechanisms are the moment tensor (MT) solutions of regular earthquakes with *Mw* of 4.3–6.5 in the F-net catalogue (Fukuyama *et al.* 1998, Kubo *et al.* 2002) that occurred in the area with latitudes less than 34.8°N, longitudes greater than 130.5°E, and at depths of less than 50 km. The periods of plotted MT solutions range from April 2004 to August 2019. The blue hatched areas represent the expected source region of the Nankai and Tonankai earthquakes (Earthquake Research Committee, 2001, available at: http://www.jishin.go.jp/main/chousa/01sep_nankai/index.htm). The earthquake marked A is the *Mw* 5.8 southeast off Kii Peninsula earthquake that occurred on 1 April 2016.

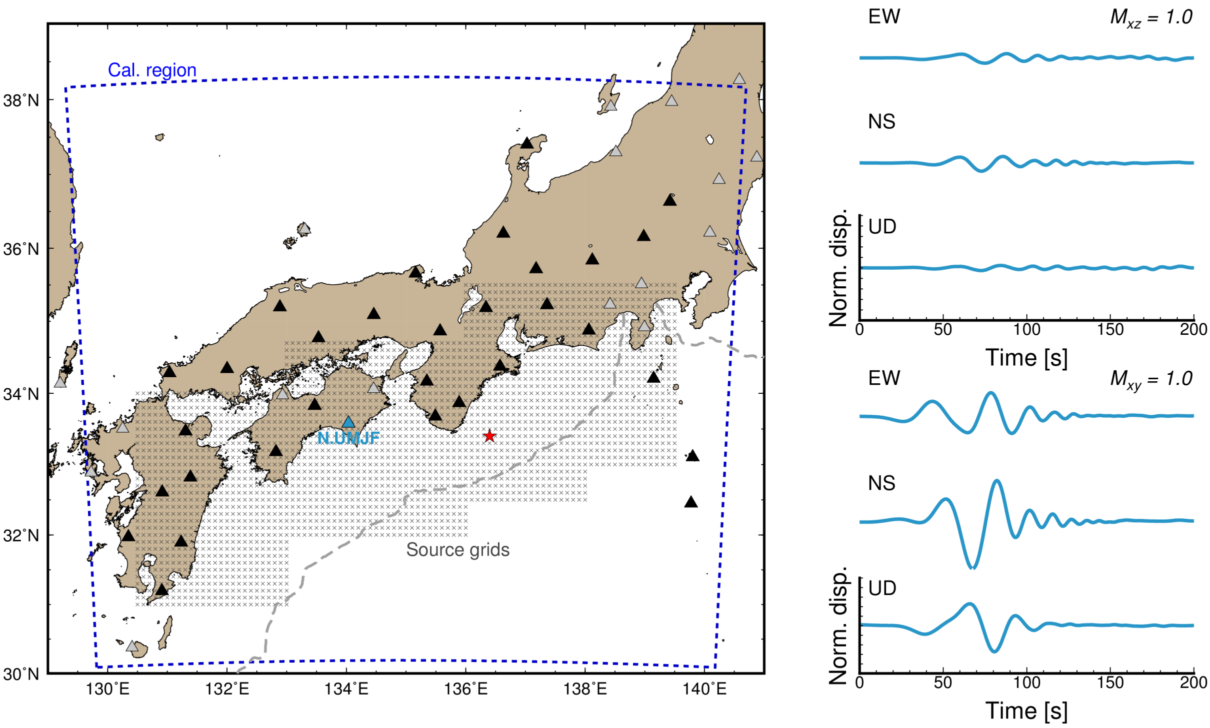

Figure 2. Calculation settings used in the study were the blue dashed line represents the horizontal coverage of the simulation model region. The triangles and crosses in the map denote the locations of the F-net stations and the assumed source grids, respectively. Green's functions from the source grids to the black-fill and blue-fill triangles were evaluated via reciprocal calculations using OpenSWPC code (Maeda *et al.* 2017). The right-hand panels show examples of filtered displacements of Green's functions from a certain hypocentre (red star) to the N.UMJF station (blue triangle). The filter passed band ranged from 25 to 100 s.

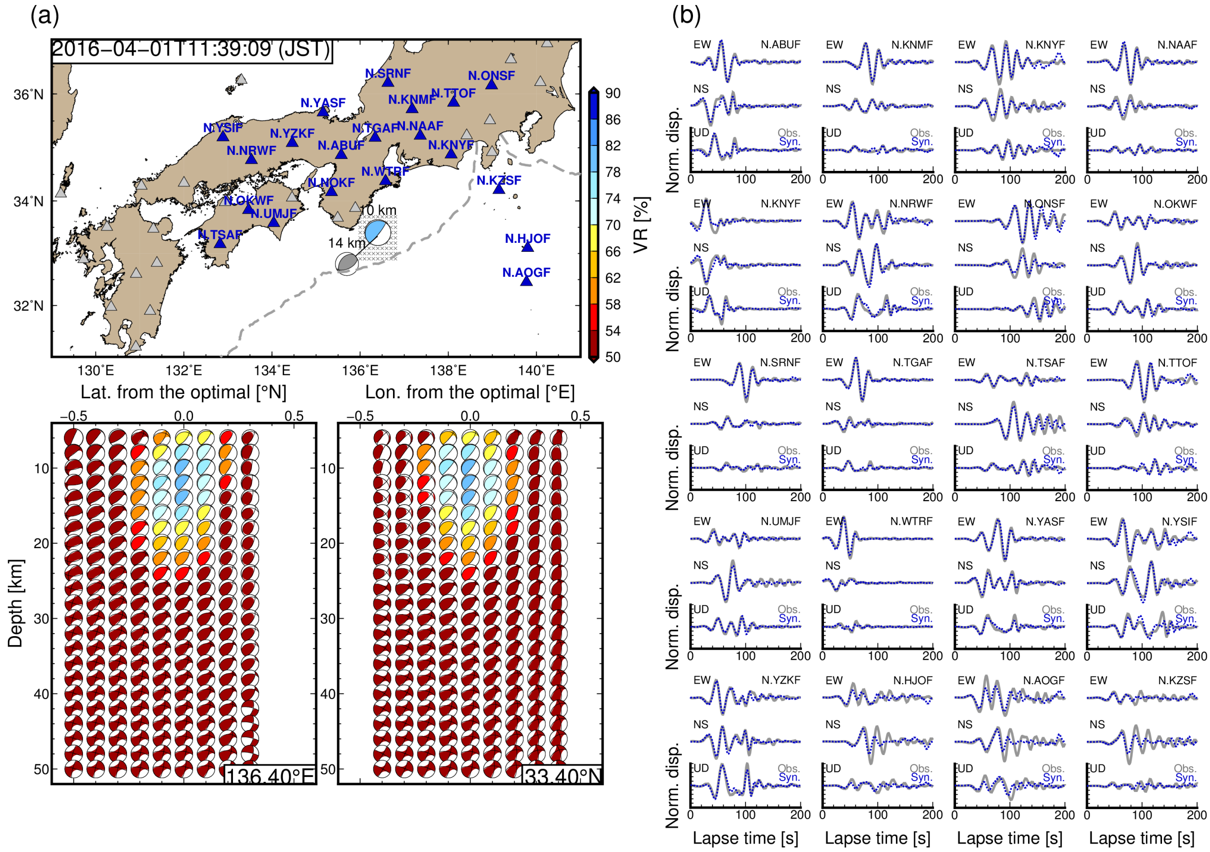

Figure 3. CMT results for the southeast off Kii Peninsula earthquake that occurred on 1 April 2016. (a) Locations of the optimal solutions, used stations, and depth variations of optimal solutions at each source grid. Colours of the focal mechanisms reflect values of variance reduction between observed and synthetic displacements for 25–100 s periods. The numbers above the optimal solutions in (a) are the optimal centroid depths. The grey focal mechanism in (a) is the F-net MT solution of this earthquake. (b) Comparisons of observed and synthetic displacements for 25–100 s periods. Grey solid and blue dotted lines are the observed and synthetic seismograms, respectively. Synthetic seismograms were evaluated by assuming the optimal solution. Amplitudes of both observed and synthetic seismograms at each station were normalised by the maximum amplitude of the observed and synthetic filtered displacements. Detailed source parameters are listed in Table S1.

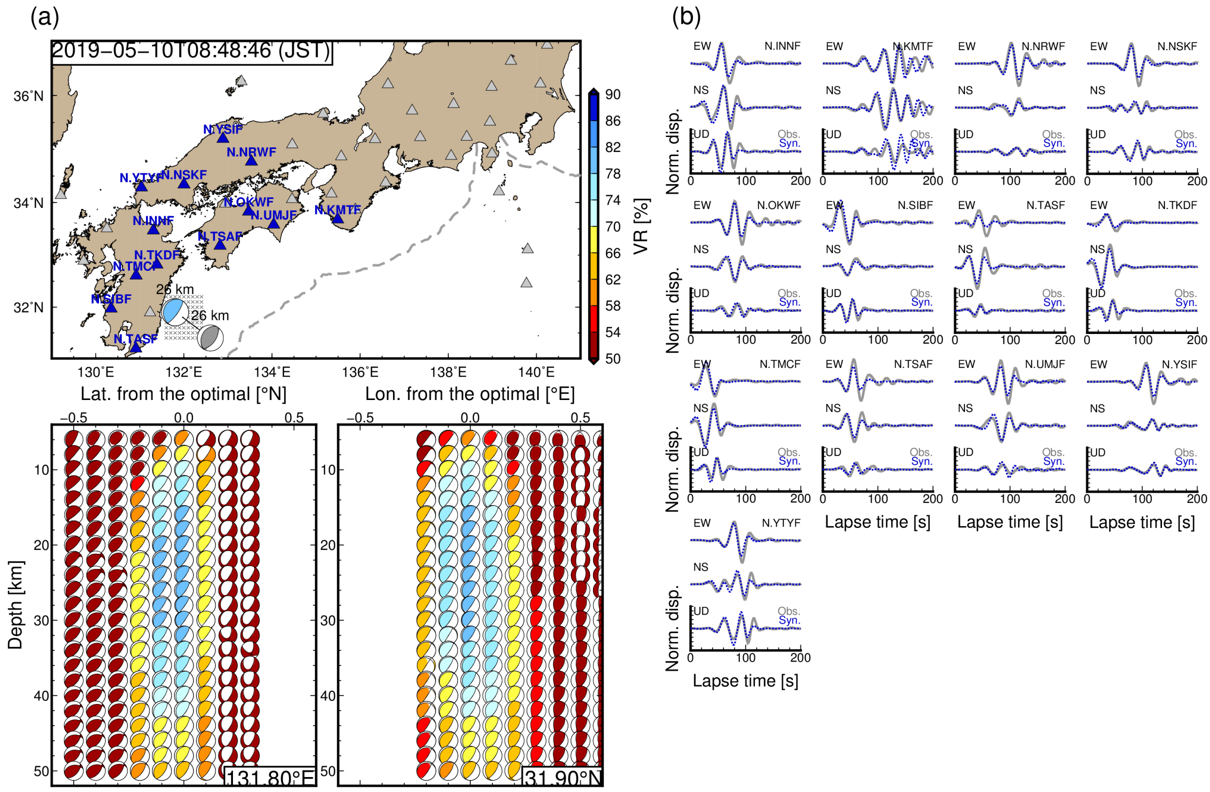

Figure 4. CMT results for the Hyuga-nada earthquake that occurred on 10 May 2019. (a) Locations of the optimal solutions, used stations, and depth variations of optimal solutions at each source grid. Colours of the focal mechanisms reflect values of variance reduction between observed and synthetic displacements for 25–100 s periods. The numbers above the optimal solutions in (a) are the optimal centroid depths. The grey focal mechanism in (a) is the F-net MT solution of this earthquake. (b) Comparisons of observed and synthetic displacements for 25–100 s periods. Grey solid and blue dotted lines are the observed and synthetic seismograms, respectively. Synthetic seismograms were evaluated by assuming the optimal solution. Amplitudes of both observed and synthetic seismograms at each station were normalised by the maximum amplitude of the observed and synthetic filtered displacements. Detailed source parameters are listed in Table S1.

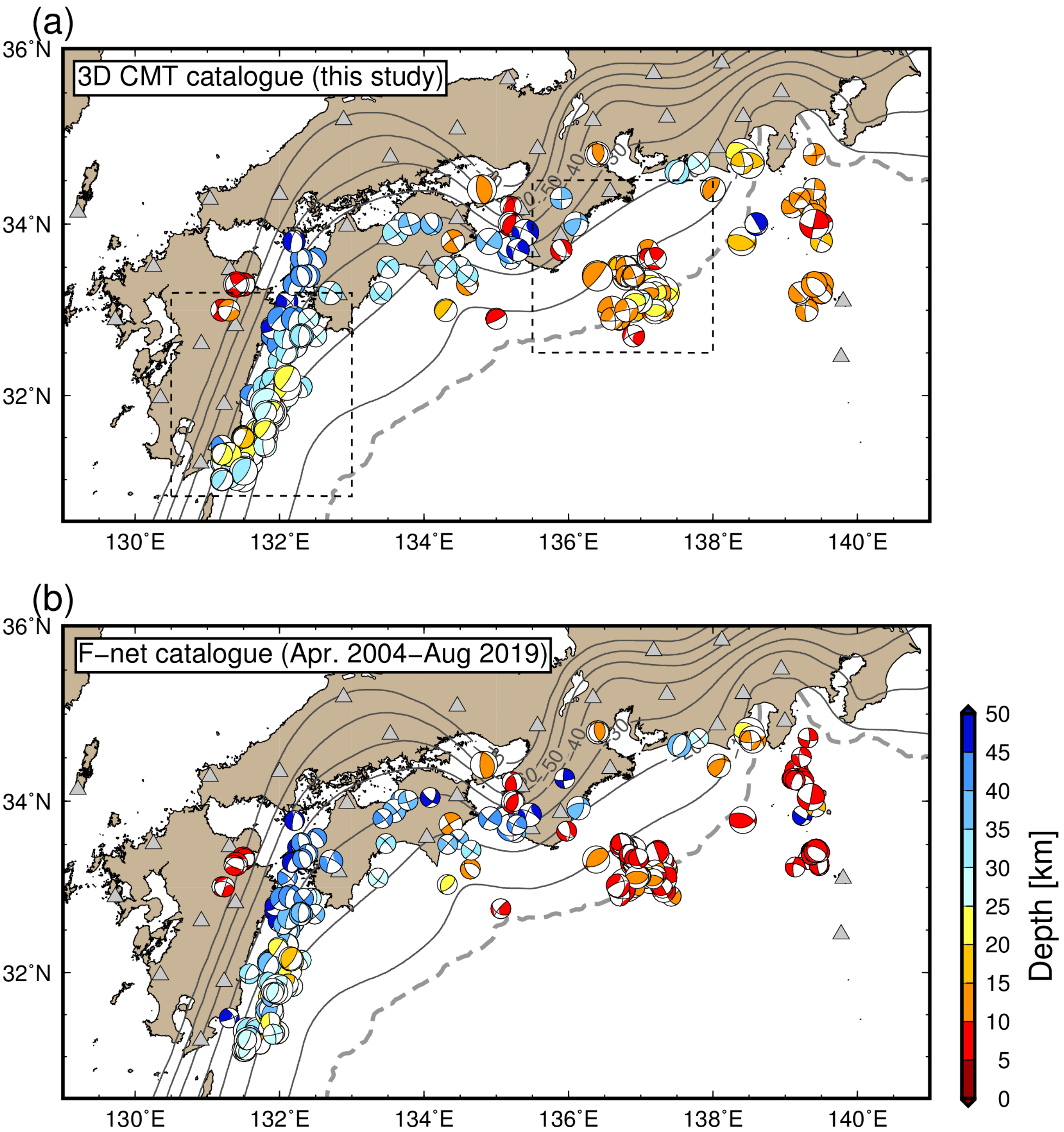

Figure 5. Comparisons of estimated CMT solutions between the (a) 3D CMT and (b) F-net MT catalogues. Colours of focal mechanisms represent the centroid depths of each solution. Detailed source parameters of our 3D CMT solutions are listed in Table S1. The regions enclosed by the dashed lines in (a) are enlarged in Figures 6 and 7.

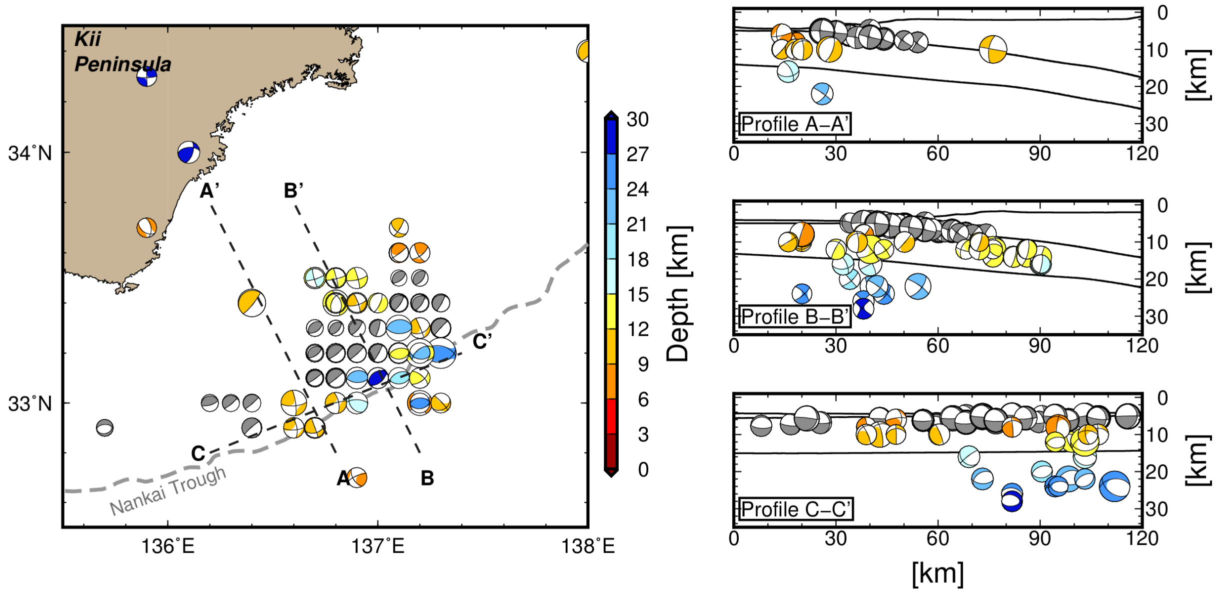

Figure 6. Spatial distribution of the CMT solutions southeast of the Kii Peninsula. Coloured focal mechanisms are our CMT solutions. Grey focal mechanisms are the CMT solutions of shallow VLFEs (Takemura, Matsuzawa, *et al.* 2019). The right-hand panels show cross-sections along profiles A-A', B-B' and C-C'. The bathymetry of ETOPO1 (Amante & Eakins 2009), the upper surface, and oceanic Moho of the Philippine Sea Plate (Koketsu *et al.* 2012) along each profile are plotted in the right-hand panels.

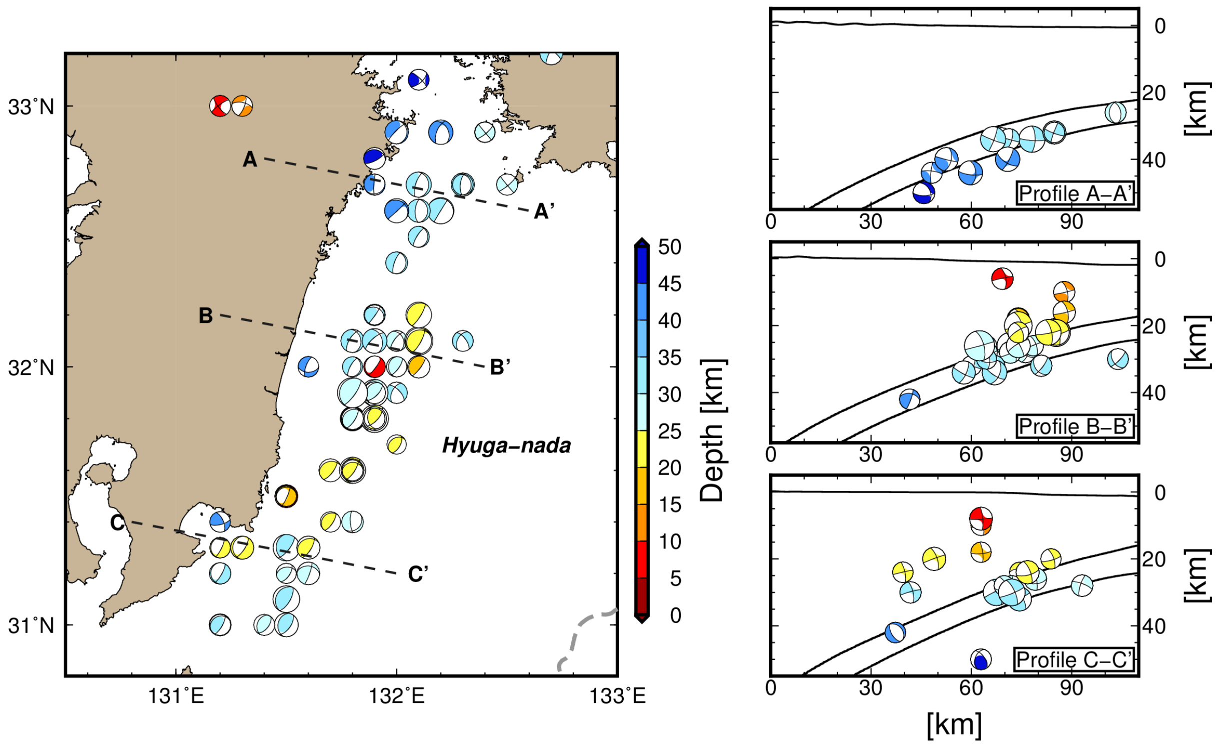

Figure 7. CMT results for the Hyuga-nada region. Coloured focal mechanisms are our CMT solutions. The right-hand panels show cross-sections along profiles A-A', B-B' and C-C'.

The bathymetry of ETOPO1 (Amante & Eakins 2009), the upper surface, and oceanic Moho of the Philippine Sea Plate (Koketsu *et al.* 2012) along each profile are plotted in the right-hand panels.

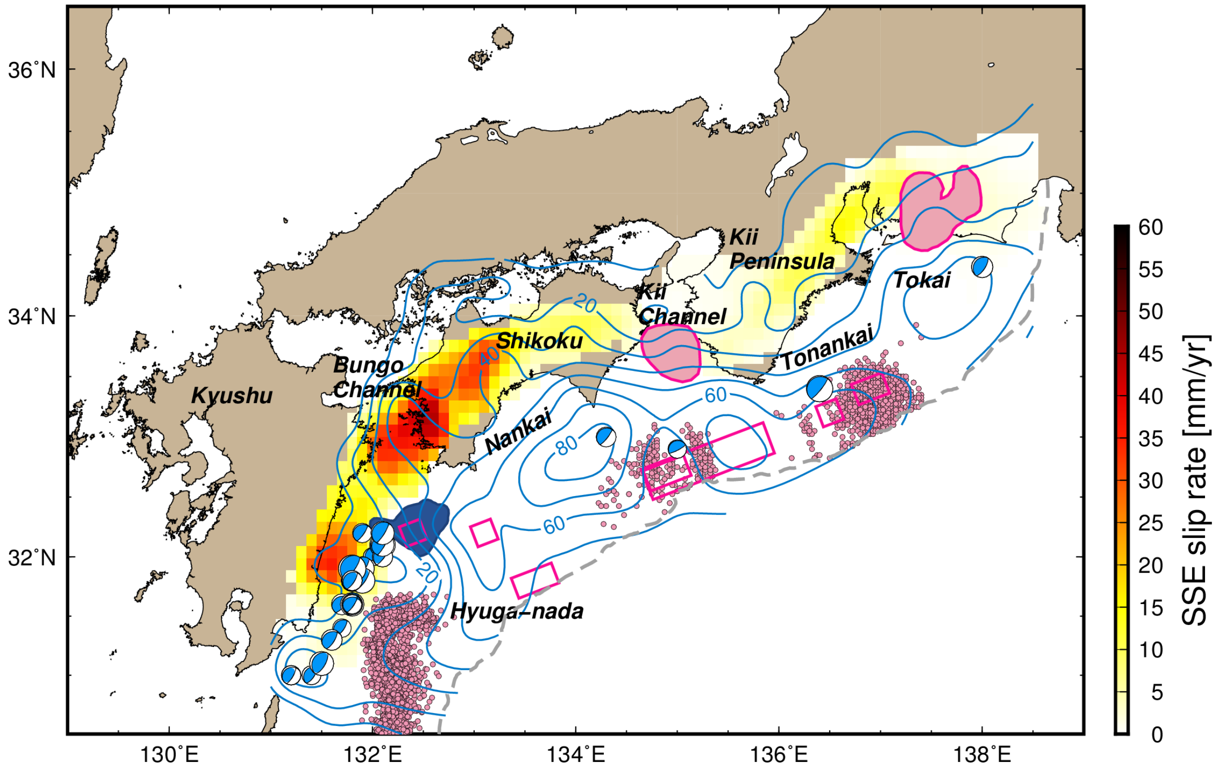

Figure 8. Spatial distribution of slip behaviours on the plate boundary along the Nankai Trough. Plotted focal mechanisms are low-angle thrust faulting solutions at depths around the plate boundary. The coseismic slip area of the 1968 *Mw* 7.5 Hyuga-nada earthquake (Yagi *et al.* 1998) is shaded in dark blue. SSE slip rates were evaluated from the combined SSE catalogues (Nishimura *et al.* 2013, Takagi *et al.* 2016, 2019). The pink circles indicate the epicentres of the shallow LFTs of the Hyuga-nada and the shallow VLFEs in the Tonankai region referred from Yamashita et al. (2015) and Takemura, Noda, et al. (2019). The pink shaded and enclosed areas indicate the large slip areas of long-term SSEs (Miyazaki *et al.* 2006, Kobayashi 2014) and shallow SSEs (Yokota & Ishikawa 2019), respectively. The blue contour lines indicate the slip-deficit rates [mm/yr] on the plate boundary by Noda *et al.* (2018)

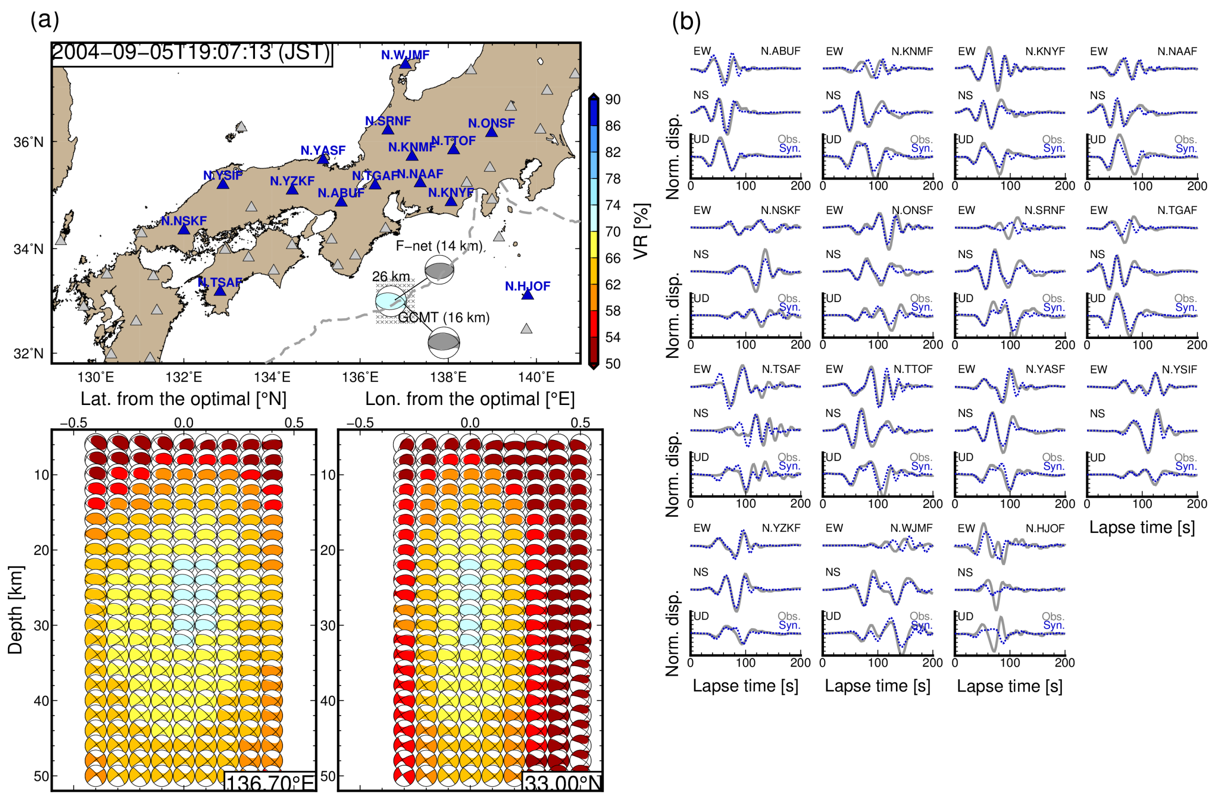

Figure 9. CMT results for the *Mw* 7.2 southeast off the Kii Peninsula earthquake that occurred on 5 September 2004. Grey focal mechanisms are the solutions of the F-net MT and GCMT catalogues. (a) Locations of the optimal solutions, used stations, and depth variations of optimal solutions at each source grid. Colours of the focal mechanisms reflect values of variance reduction between observed and synthetic displacements for 25–100 s periods. The numbers above the optimal solutions in (a) are the optimal centroid depths. The grey focal mechanism in (a) is the F-net MT solution of this earthquake; (b) Comparisons of observed and synthetic displacements for 25–100 s periods. Grey solid and blue dotted lines are the observed and synthetic seismograms, respectively. Synthetic seismograms were evaluated by assuming the optimal solution. Amplitudes of both observed and synthetic seismograms at each station were normalised by the maximum amplitude of the observed and synthetic filtered displacements. Detailed source parameters are listed in Table S2.

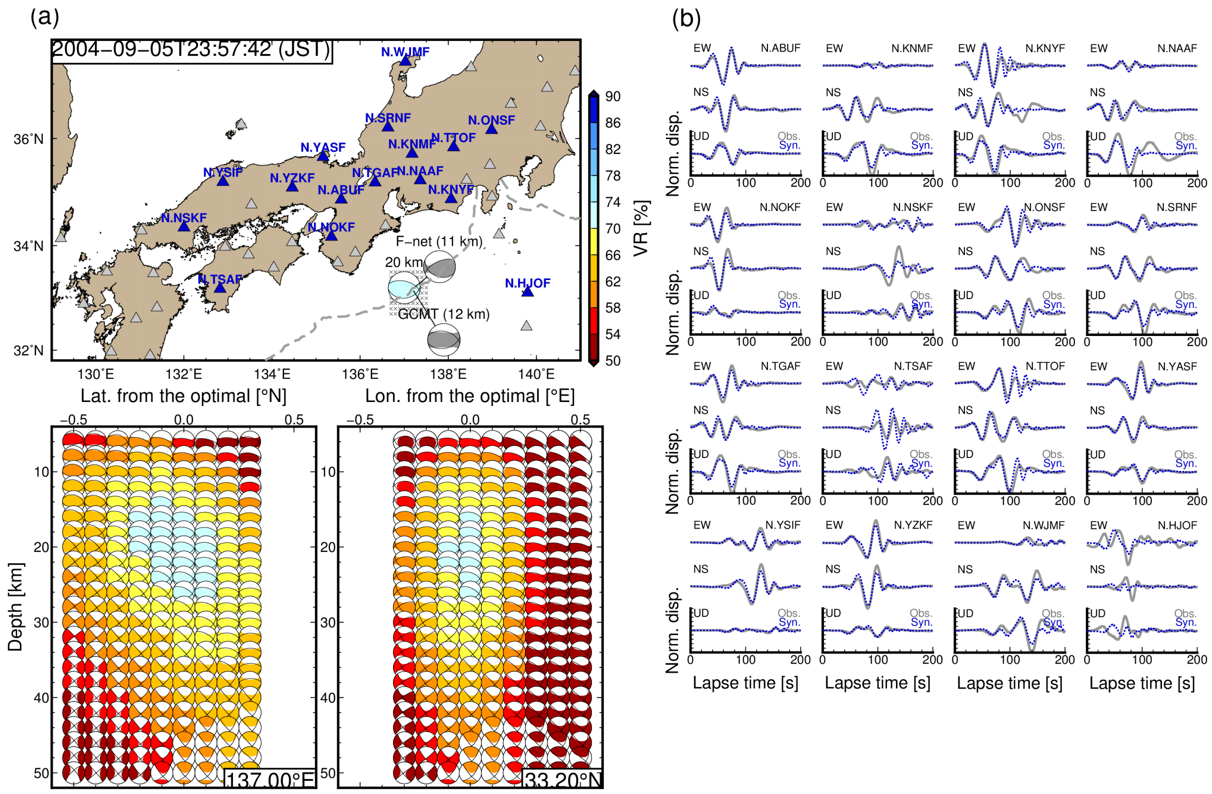

Figure 10. CMT results for the *Mw* 7.5 southeast off the Kii Peninsula earthquake that occurred on 5 September 2004. (a) Locations of the optimal solutions, used stations, and depth variations of optimal solutions at each source grid. Colours of the focal mechanisms reflect values of variance reduction between observed and synthetic displacements for 25–100 s periods. The numbers above the optimal solutions in (a) are the optimal centroid depths. The grey focal mechanism in (a) is the F-net MT solution of this earthquake; (b) Comparisons of observed and synthetic displacements for 25–100 s periods. Grey solid and blue dotted lines are the observed and synthetic seismograms, respectively. Synthetic seismograms were evaluated by assuming the optimal solution. Amplitudes of both observed and synthetic seismograms at each station were normalised by the maximum amplitude of the observed and synthetic filtered displacements. Detailed source parameters are listed in Table S2.

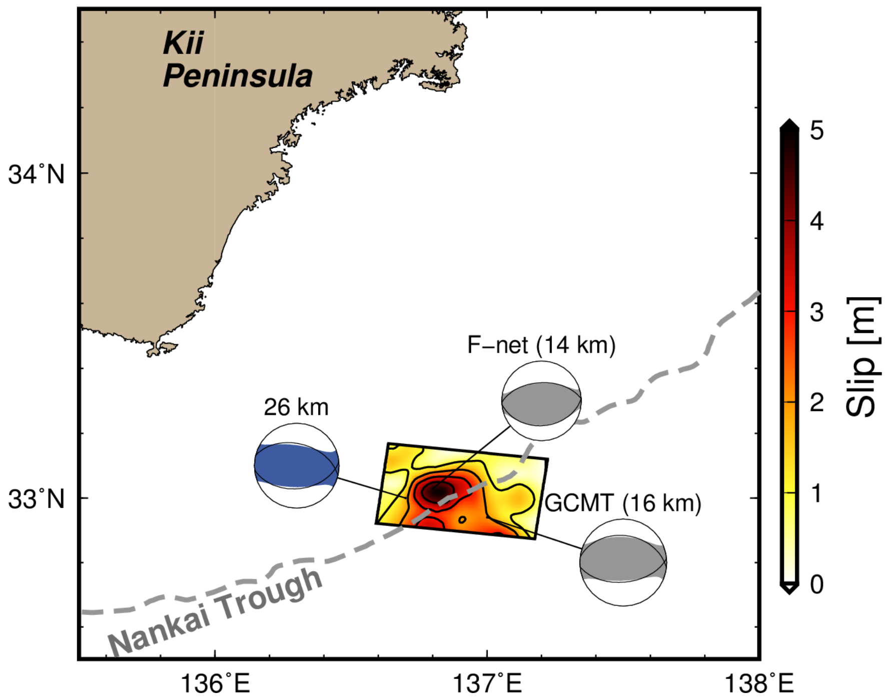

Figure 11. Comparison of the CMT results for the *Mw* 7.2 southeast off the Kii Peninsula earthquake and other CMT catalogues (Fukuyama *et al.* 1998, Kubo *et al.* 2002, Ekström *et al.* 2012) and finite fault modelling (Okuwaki & Yagi 2018) solutions.

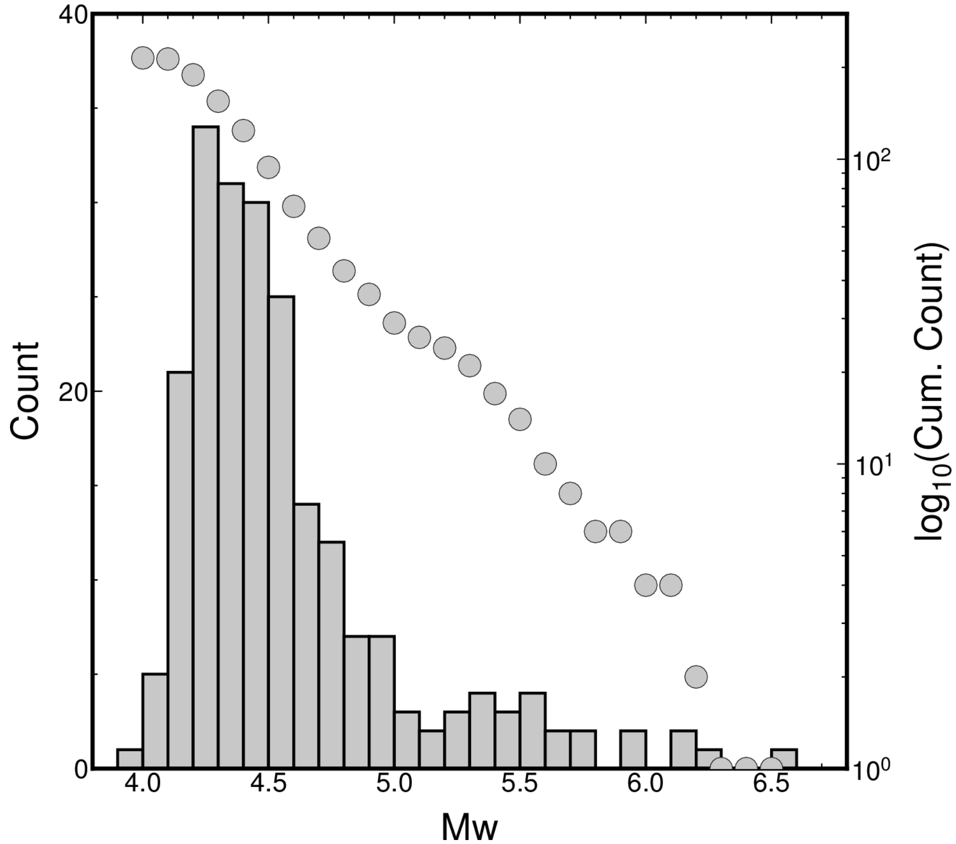

Figure S1. Size distribution of our 3D CMT catalogue.

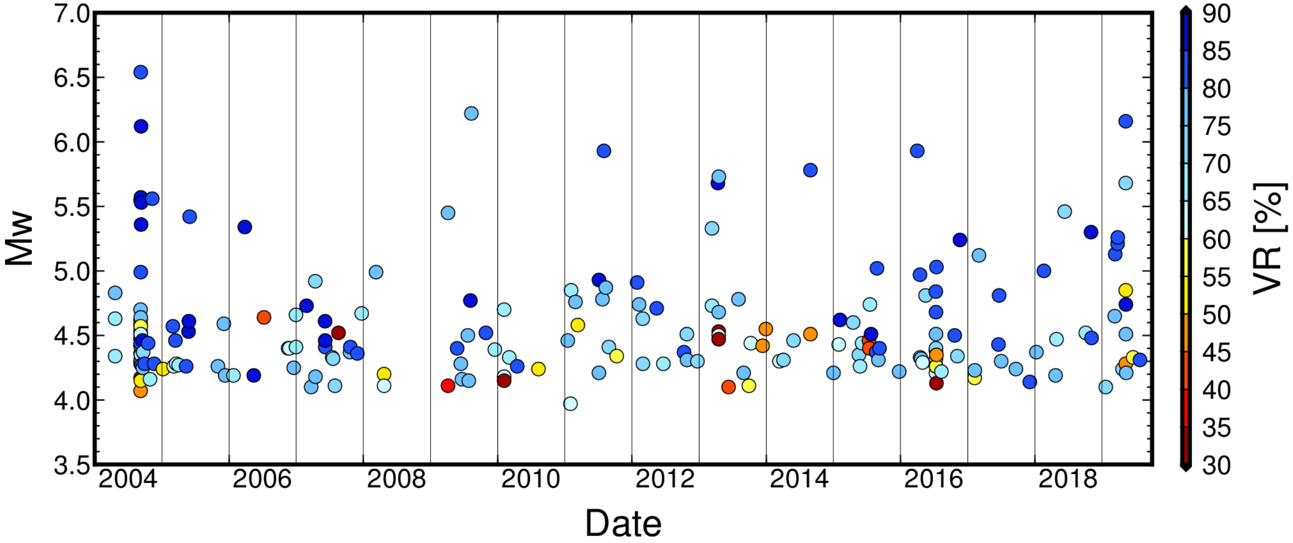

Figure S2. Magnitude-time diagram of our 3D CMT catalogue.

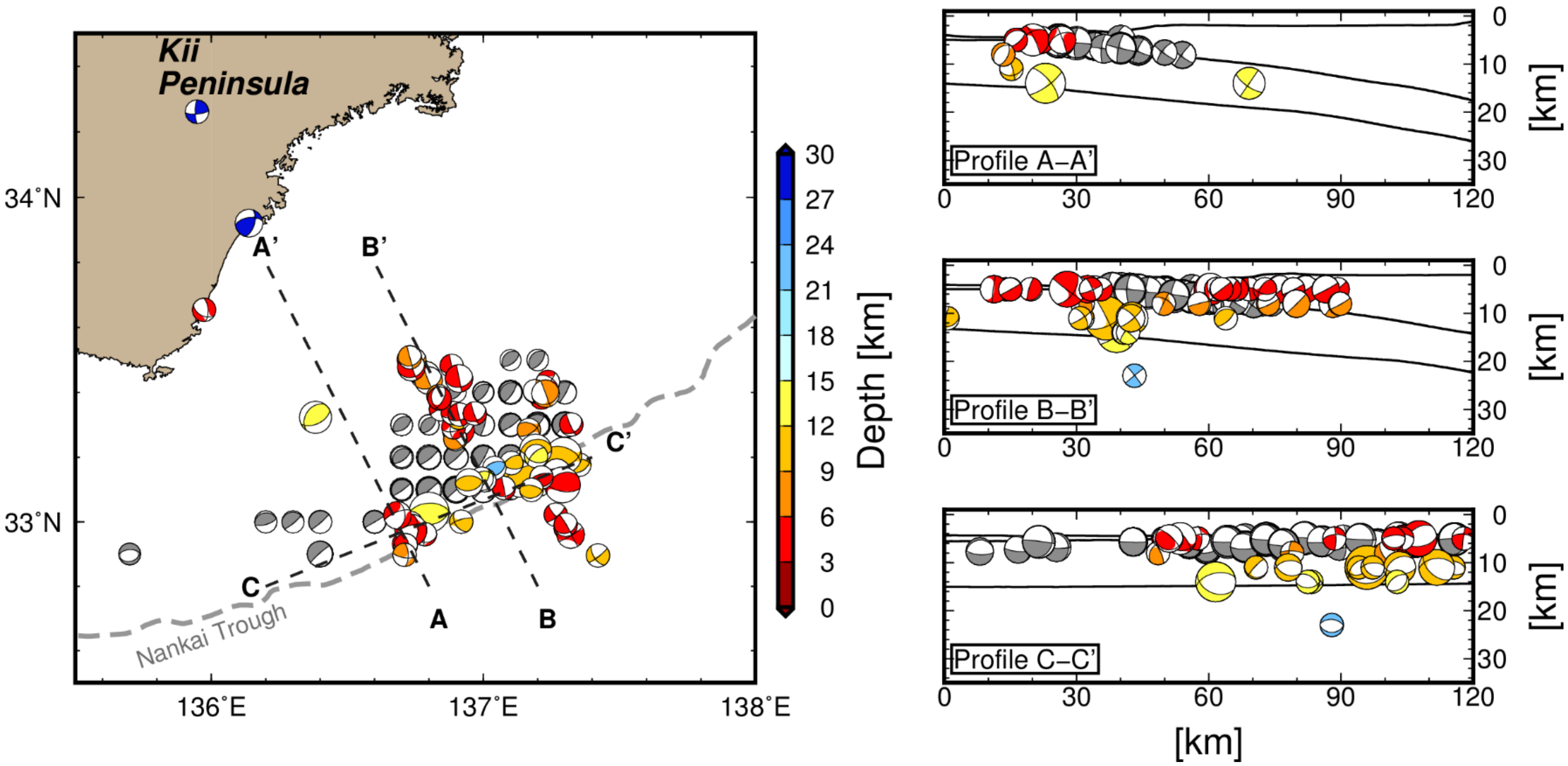

Figure S3. Spatial distribution of CMT solutions southeast of the Kii Peninsula. Coloured focal mechanisms are referenced from the F-net MT catalogue. Grey focal mechanisms are the CMT solutions of shallow VLFEs (Takemura, Matsuzawa et al., 2019). Right-hand panels show cross-sections along profiles of A, B and C. The bathymetry of ETOPO1 (Amante & Eakins, 2009), the upper surface, and the oceanic Moho of the Philippine Sea Plate (Koketsu et al., 2012) along each profile are plotted in the right-hand panels.

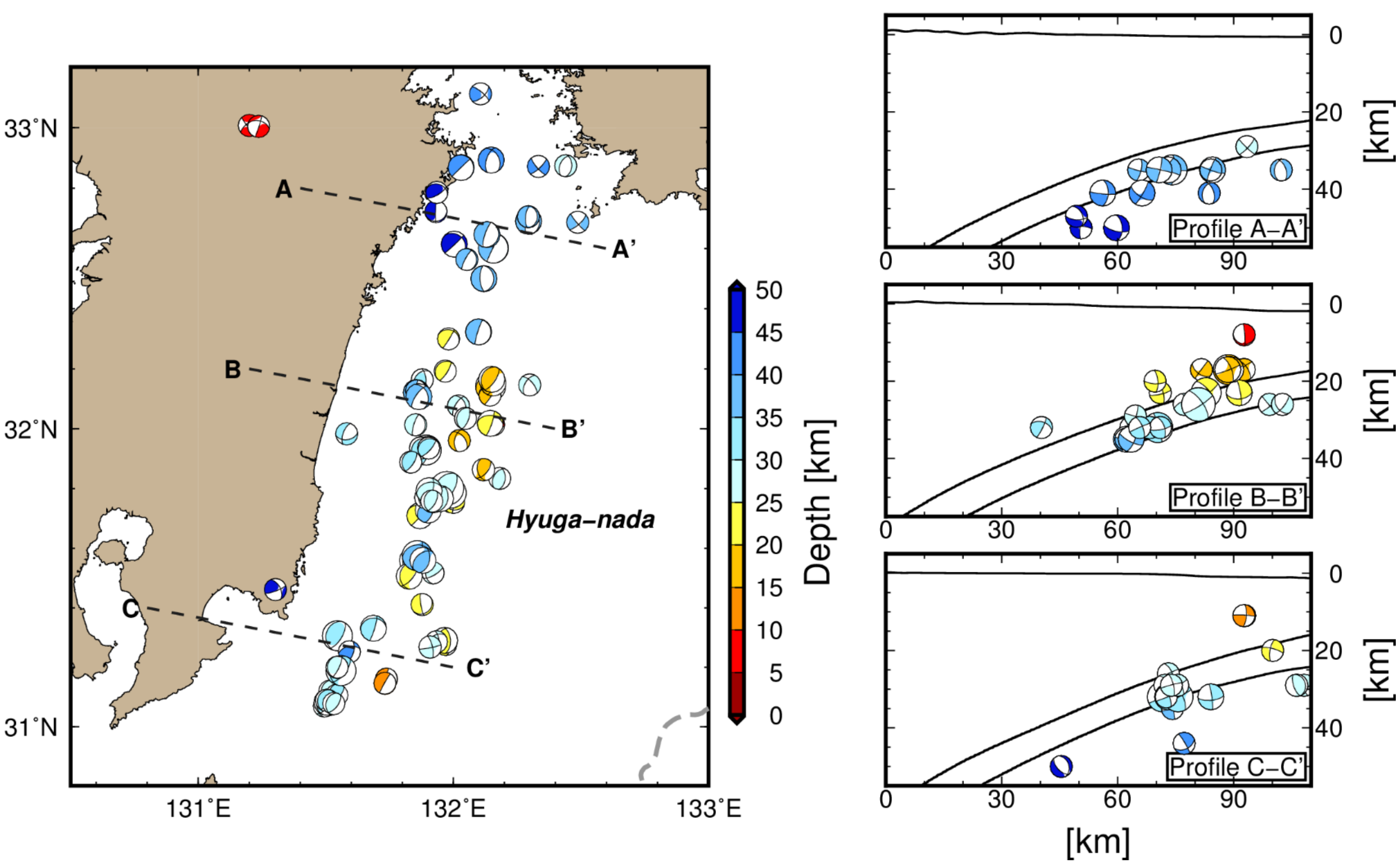

Figure S4. CMT results for the Hyuga-nada region.

Table S1. CMT solutions for all analysed moderate earthquakes.

Centroid time (JST)	Lon.	Lat.	Depth [km]	M_{rr}	$M_{\theta\theta}$	$M_{\phi\phi}$	$M_{r\theta}$	$M_{r\phi}$	$M_{\theta\phi}$	Exp.	Mw	VR [%]
2004-04-20T22:26:31	132.3	33.5	38	-1.357	-1.6975	3.0545	-2.4812	-1.2316	1.3686	22	4.34	67.5
2004-04-21T12:10:42	131.8	31.6	20	0.6864	-0.0375	-0.6489	0.5203	0.6678	-0.2541	23	4.63	68.2
2004-04-21T12:20:53	131.8	31.5	24	1.4508	0.101	-1.5519	0.7083	1.1275	-0.88	23	4.83	78.5
2004-09-06T05:31:03	136.8	33.4	12	0.1901	-1.3058	1.1157	0.5788	0.5214	2.1794	24	5.55	82.9
2004-09-06T07:48:43	137.1	33.1	20	8.4568	-8.4845	0.0277	-0.1917	-2.1778	-2.2808	22	4.57	35.9
2004-09-06T08:59:38	136.9	33.5	14	0.0678	-0.5335	0.4657	0.0528	0.2794	0.9021	23	4.62	72
2004-09-06T11:06:49	137.1	33.6	8	0.3185	1.9433	-2.2618	2.1684	1.7754	-0.2504	22	4.3	65.6
2004-09-06T11:45:40	137.2	33	10	0.2274	-1.8402	1.6128	-1.0266	-0.1838	1.0249	22	4.17	34.7
2004-09-06T13:49:06	136.8	33.4	14	-0.1743	-0.7335	0.9078	-0.4744	0.9627	0.8908	22	4.07	46.5
2004-09-06T13:59:29	136.8	33.5	12	0.0023	-3.4627	3.4604	-0.5306	1.2586	3.9296	22	4.42	77.3
2004-09-06T14:28:53	136.8	33.5	14	0.3208	-2.9967	2.6759	-1.0328	1.7334	2.6699	22	4.36	61.5
2004-09-06T15:35:46	137	33.1	8	0.4137	-2.4345	2.0208	-0.3197	3.3327	3.4922	22	4.42	66
2004-09-06T15:46:49	136.8	33.5	14	0.2543	-4.7452	4.4909	-1.6442	3.1665	4.4559	22	4.51	74.4
2004-09-06T15:54:36	136.7	33.5	16	0.0747	-7.0077	6.933	-1.2333	2.2972	6.3312	22	4.59	80.5
2004-09-06T16:10:06	136.8	33.4	14	0.0901	-3.5793	3.4892	-2.0548	3.9333	3.2224	22	4.48	77.4
2004-09-06T17:20:33	137.3	33.2	24	5.9227	-6.1459	0.2233	-1.5096	0.6317	-1.4292	22	4.47	76.1
2004-09-06T18:11:58	136.9	33	16	0.8177	-1.054	0.2362	-0.7249	-0.0274	0.754	23	4.7	78.6
2004-09-06T19:29:19	137.1	33.2	24	6.406	-8.5764	2.1704	1.9059	-0.0017	-0.7362	22	4.53	68.2
2004-09-06T19:39:48	137.2	33.1	12	1.8829	-5.3833	3.5004	-0.1144	3.0965	0.3394	22	4.44	81.5
2004-09-06T19:59:33	136.6	32.9	8	0.4562	-1.5261	1.07	1.2246	-0.9694	2.5349	22	4.28	59.1
2004-09-07T01:45:30	136.7	33.5	14	-0.0595	-0.7935	0.8531	-0.1833	0.3445	0.6876	23	4.64	78.2

2004-09-07T02:23:38	136.7	32.9	6	0.2361	-0.1379	-0.0982	4.0372	7.3778	3.1622	22	4.57	57
2004-09-07T05:02:49	136.7	33.5	16	-0.0954	-0.7284	0.8238	-0.2423	0.194	1.227	22	4.05	59.4
2004-09-07T08:29:42	137.3	33.2	24	6.76	-8.7612	2.0012	-1.4126	1.3995	-0.0672	25	6.54	81.4
2004-09-07T15:10:05	137.2	33.2	16	3.072	-2.8076	-0.2643	-2.2188	-0.1924	-0.9517	23	4.99	82.9
2004-09-07T15:17:51	137.1	33.7	10	0.3662	1.3792	-1.7454	0.9704	0.8069	0.5912	22	4.15	51.8
2004-09-07T19:58:54	137.2	33.3	10	-0.0713	-3.9503	4.0216	-0.3628	4.9111	3.4998	22	4.51	63.1
2004-09-07T20:56:31	137	33.4	12	-1.194	-1.0187	2.2127	-1.0691	-2.4823	1.6183	22	4.31	42.5
2004-09-08T02:20:25	136.9	32.7	6	0.1269	-2.5415	2.4145	-1.2574	-2.5651	1.8652	22	4.35	67.8
2004-09-08T03:36:24	137.1	33.3	22	2.6349	-2.7037	0.0688	0.8996	-0.2034	-0.1734	24	5.57	85.1
2004-09-08T06:02:15	137.1	33.6	8	0.5073	0.5042	-1.0115	1.6876	0.7738	0.0002	22	4.14	57.6
2004-09-08T23:40:11	137.2	33	8	0.2604	-1.2801	1.0197	-0.4993	0.2195	0.5308	24	5.36	85.9
2004-09-08T23:58:28	137.2	33.2	12	1.4523	-2.0393	0.587	-0.3272	-0.3446	-0.2475	25	6.12	89.3
2004-09-10T11:05:58	136.6	33	10	0.0174	-0.49	0.4726	0.4933	0.9044	2.1698	24	5.53	86.9
2004-09-11T18:05:59	136.7	32.9	10	0.0774	-1.539	1.4616	-0.5858	2.0363	1.9158	22	4.27	83.4
2004-09-17T03:56:29	136.6	32.9	10	-0.6156	-0.5277	1.1433	2.849	3.2868	4.2744	22	4.46	87
2004-09-18T09:48:39	136.8	33.5	12	-0.3511	-1.1663	1.5174	0.16	0.4742	2.562	22	4.25	77.3
2004-09-20T05:17:52	137.2	33.6	8	0.7036	3.2305	-3.9341	2.1988	-0.4975	-1.371	22	4.37	74.1
2004-09-28T00:37:44	137.3	33	10	0.572	-1.861	1.289	-2.1759	1.1947	1.3091	22	4.28	83
2004-10-03T08:00:21	136.8	33.4	12	-1.4439	-0.6286	2.0725	0.4632	0.2373	0.1244	22	4.12	71.9
2004-10-17T07:05:42	137.2	33.2	22	3.9515	-5.1385	1.187	-1.2903	-2.6526	-1.8995	22	4.44	82
2004-10-27T21:27:31	135.2	33.6	34	-0.4372	-1.7282	2.1655	0.0469	-0.4457	-0.8677	22	4.16	69.7
2004-11-09T00:07:28	138.4	33.8	16	2.1695	-2.6496	0.4801	-1.013	0.6477	0.3658	24	5.56	82.9
2004-11-19T05:46:28	137.1	33.2	12	2.9056	-3.3445	0.4389	-0.7283	-0.4218	-0.4779	22	4.28	80.9
2005-01-05T23:49:13	139.3	34.2	8	1.2691	-3.1909	1.9218	0.0929	0.5325	0.6501	22	4.24	53.4

2005-03-01T06:59:46	136.9	33.4	12	1.001	-5.8171	4.8162	3.1308	1.8919	6.0684	22	4.57	84.1
2005-03-05T14:58:50	131.2	31.4	42	0.8974	-2.0131	1.1156	0.8395	1.2316	2.0335	22	4.26	65
2005-03-14T19:49:32	137	33.1	28	5.7175	-4.7523	-0.9652	-2.4026	-0.055	-2.0364	22	4.46	82.3
2005-03-19T11:34:10	137.2	33	24	2.9604	-3.5697	0.6093	-0.3674	0.0348	-0.3644	22	4.28	64.7
2005-04-01T09:41:49	131.4	31	32	2.3644	-0.8107	-1.5537	1.1653	1.8244	-1.0436	22	4.27	68.1
2005-05-12T04:22:51	132	32.1	28	-1.6099	-1.0197	2.6296	1.3696	1.5371	0.5932	22	4.26	82.7
2005-05-25T20:31:30	132.3	33.4	46	-3.1031	-4.2984	7.4014	3.3402	2.2254	-1.7336	22	4.53	85.3
2005-05-27T03:17:19	133.7	34	36	-0.4494	-0.5497	0.9991	-0.4676	-0.3466	0.0844	23	4.61	89.6
2005-05-31T11:04:15	131.5	31.3	30	0.9813	0.0704	-1.0517	0.9508	0.8888	-0.3208	24	5.42	81
2005-11-01T12:47:35	135.1	33.8	46	-1.0601	0.5529	0.5072	-2.2706	-1.4095	1.1458	22	4.26	78.4
2005-12-03T10:39:02	137	33.1	26	10.1208	-7.3714	-2.7493	0.143	0.8015	-3.3126	22	4.59	77.6
2005-12-03T11:01:22	137	33.1	28	6.9856	-4.731	-2.2546	1.1887	1.4634	-4.1805	22	4.52	73.3
2005-12-10T18:32:09	132	32	26	1.4435	-0.1028	-1.3406	1.2512	1.4464	-0.4202	22	4.19	76.2
2006-01-24T21:36:47	131.7	31.4	20	1.4303	-0.585	-0.8453	1.0039	1.6058	-0.7574	22	4.19	67.2
2006-03-27T11:50:26	132.2	32.6	34	-0.0067	-0.2097	0.2164	0.662	1.1059	-0.028	24	5.34	86.6
2006-05-15T01:42:11	135.2	34.2	6	1.4901	1.0789	-2.569	-0.0809	0.6344	-0.7802	22	4.19	86.2
2006-07-09T17:48:06	139.4	34.3	14	0.2085	-0.7853	0.5769	-0.0862	0.1949	-0.8847	23	4.64	40.9
2006-11-18T01:08:36	132	31.9	32	-2.5129	-2.3879	4.9008	2.409	-0.5069	-1.1892	22	4.4	75.1
2006-11-25T15:39:45	132.1	32	10	2.5354	-0.9052	-1.6302	2.6184	3.5397	-0.3243	22	4.4	60.1
2006-12-19T03:28:50	131.6	32	42	-1.3385	1.3769	-0.0384	-0.1348	1.8295	1.909	22	4.25	79.2
2006-12-31T02:49:32	139.4	34.2	12	-0.4855	-0.0157	0.5012	-0.615	0.1021	-0.9646	23	4.66	67.2
2006-12-31T03:42:11	139.3	34.2	12	-3.5025	2.406	1.0965	1.3953	-0.4392	-3.8411	22	4.41	69
2007-02-25T20:41:22	136.9	33.1	22	1.4403	-1.4342	-0.0061	0.6018	-0.234	-0.1851	23	4.73	85.6
2007-03-23T16:20:53	136.9	33.4	10	0.0059	-0.9814	0.9755	0.2088	0.6617	1.3486	22	4.1	76.6

2007-04-15T12:19:29	136.4	34.8	14	2.738	-0.2696	-2.4684	0.5046	0.7611	1.2386	23	4.92	71.7
2007-04-15T18:34:45	136.4	34.8	12	1.9049	0.3127	-2.2177	0.8835	-0.5492	0.1329	22	4.18	77.1
2007-04-26T09:02:55	133.6	33.9	34	0.4223	-3.5005	3.0782	-0.3535	0.9473	0.6558	23	4.96	88.6
2007-06-06T23:42:49	131.5	33.3	10	-0.2061	0.9777	-0.7716	0.0837	0.3929	-0.2776	23	4.61	87.3
2007-06-07T17:22:15	131.5	33.3	8	-1.5836	5.0032	-3.4196	0.3935	2.2127	-1.7062	22	4.41	84.5
2007-06-07T20:50:39	131.5	33.3	8	-2.1527	5.917	-3.7642	-0.8056	2.8071	-1.6272	22	4.46	85.8
2007-07-16T17:24:18	135.9	34.3	38	-0.1656	0.321	-0.1555	0.1414	-0.7578	-3.897	22	4.33	61.3
2007-07-20T17:15:25	139.4	34.8	12	1.0774	0.0622	-1.1396	-1.0415	-1.0824	-3.2583	22	4.32	71.5
2007-07-31T10:22:40	131.9	32.2	26	1.4741	0.1401	-1.6142	-0.2327	0.8087	-0.4541	22	4.11	70.2
2007-08-19T10:21:55	138.6	34	50	-0.8675	2.5606	-1.6931	3.3543	-6.004	-2.0221	22	4.52	31.5
2007-10-21T02:09:27	131.9	32.2	28	2.0351	-1.1698	-0.8653	2.1099	3.2966	-1.3251	22	4.37	76.8
2007-10-22T09:36:00	139.1	34.2	14	2.3922	-4.9035	2.5113	-1.501	2.5717	0.6986	22	4.41	83
2007-11-29T20:17:48	131.9	32.7	44	-0.1989	-1.1422	1.3411	0.5946	4.0001	1.1751	22	4.36	83.3
2007-12-23T02:49:06	131.6	31.2	26	0.3196	-0.4838	0.1642	0.231	1.001	-0.6548	23	4.67	69.4
2008-03-10T10:44:31	131.8	31.8	18	2.1467	-0.885	-1.2617	1.7677	2.7101	-0.8194	23	4.99	75.5
2008-04-22T18:07:20	131.4	31	28	0.8657	-0.9318	0.0661	-1.2227	-1.0644	-1.7256	22	4.2	54.3
2008-04-22T18:26:11	131.5	31	24	0.5488	-0.919	0.3702	-1.0332	-0.8558	-0.9915	22	4.11	62.9
2009-04-05T18:36:28	131.9	31.9	26	1.0367	-0.2014	-0.8353	0.9717	1.2803	-0.3601	24	5.45	78.2
2009-04-05T18:53:18	131.8	31.9	28	0.613	-0.416	-0.197	0.9975	1.3747	0.4606	22	4.11	37.3
2009-05-25T20:26:21	137.8	34.7	28	0.3139	-4.7617	4.4478	-0.1079	1.6215	0.7652	22	4.4	82.6
2009-06-14T19:17:54	132.1	33.1	50	0.1692	-2.7974	2.6282	-0.3131	1.8257	0.0194	22	4.28	78.2
2009-06-20T04:22:18	135	32.9	6	0.8329	-0.6077	-0.2252	1.8332	0.9457	-0.3284	22	4.16	76.6
2009-07-22T23:51:01	134.3	33	16	2.5675	-1.5958	-0.9717	3.9223	5.157	-1.5788	22	4.5	77.4
2009-07-28T05:30:55	131.8	32	32	-1.0858	-0.0334	1.1193	0.8299	1.4609	0.5419	22	4.15	77.5

2009-08-05T12:51:14	132.1	32.6	34	-1.2827	-0.1958	1.4785	0.0996	1.1442	0.0227	23	4.77	85
2009-08-11T05:07:09	138.4	34.8	22	2.0222	-2.2667	0.2445	1.0673	0.7672	0.9577	25	6.22	79.5
2009-10-29T02:37:09	132	32.4	32	-4.0859	-0.0828	4.1687	2.26	5.8198	0.9274	22	4.52	81
2009-12-16T14:12:51	133.4	33.2	30	0.3214	-4.1432	3.8218	-2.6779	-0.1908	-0.0985	22	4.39	69.8
2010-02-04T17:41:59	131.5	31.5	10	-1.2762	0.6802	0.596	-0.9353	-1.8535	0.0247	22	4.18	61.7
2010-02-04T20:30:09	131.5	31.5	8	-0.3484	0.2543	0.0942	-0.5176	-1.2826	0.0114	23	4.7	65.3
2010-02-04T20:35:22	131.5	31.1	28	0.1496	0.5215	-0.6711	-0.5513	-1.7085	-0.907	22	4.15	33.1
2010-03-05T06:49:56	139.5	33.8	16	-0.5247	-2.8574	3.3822	0.6979	-0.0789	-2.2332	22	4.33	69.1
2010-04-17T05:34:56	132.5	33.6	40	-2.5829	0.5543	2.0287	1.3273	-0.9056	-1.1129	22	4.26	84.9
2010-08-10T21:24:07	132.4	32.9	32	-2.7518	0.121	2.6308	0.4307	-0.2828	0.8577	22	4.24	51.6
2011-01-16T20:33:23	133.8	34	36	-0.1685	-3.5513	3.7198	-0.694	0.9807	4.8382	22	4.46	78.9
2011-02-01T02:32:25	132	31.7	22	0.8643	-0.3696	-0.4947	0.2119	0.5494	-0.5995	22	3.97	62.9
2011-02-04T18:11:24	131.5	31	32	2.1193	-0.4547	-1.6646	0.9618	0.8368	-0.6417	23	4.85	68.8
2011-02-28T09:04:34	131.8	32.1	34	-1.1333	-0.2285	1.3618	0.7021	0.9012	0.3583	23	4.76	78.5
2011-03-12T22:11:02	136.8	33	10	-1.3814	-2.7719	4.1533	3.2202	1.0853	8.0288	22	4.58	52.3
2011-07-05T19:18:42	135.2	34	8	2.6477	-0.4269	-2.2208	-0.075	1.2127	-1.4264	23	4.93	86.5
2011-07-05T19:34:54	135.2	34	8	2.2075	-0.3256	-1.8819	0.1836	1.097	-1.152	22	4.21	75.3
2011-07-24T23:32:12	136.1	34	38	1.0659	-0.8068	-0.2591	-0.4365	0.8299	-1.316	23	4.78	78.5
2011-08-01T23:58:13	138.5	34.7	18	8.7245	-8.3238	-0.4008	4.6443	0.4007	0.2345	24	5.93	81.6
2011-08-12T04:37:46	138	34.4	10	1.7337	-0.545	-1.1887	1.0074	1.5403	-0.7179	23	4.87	76.4
2011-08-28T09:52:03	131.2	31	30	3.6473	-2.181	-1.4662	1.7998	3.4005	-1.3799	22	4.41	71
2011-10-10T19:19:28	134.1	34	38	-2.0054	-1.171	3.1764	-2.5103	1.3851	-0.4369	22	4.34	55.4
2012-01-30T03:18:21	132	32.6	44	0.177	-0.8981	0.7212	2.0799	1.8079	-0.2874	23	4.91	84.5
2012-02-09T12:55:15	131.6	31.3	24	1.0229	-0.6082	-0.4147	0.5156	1.1158	-0.6235	23	4.74	77.6

2012-02-29T01:23:02	131.9	31.8	18	0.6718	-0.1089	-0.5629	0.5605	0.6858	-0.202	23	4.63	70.7
2012-02-29T19:33:33	131.8	31.6	18	1.0949	0.179	-1.2738	1.1601	2.8352	0.0018	22	4.28	73
2012-05-14T12:36:44	131.7	31.6	24	0.8837	-0.634	-0.2497	0.5745	0.9543	-0.5517	23	4.71	82.8
2012-06-20T03:35:33	132.3	32.1	30	-1.8684	-1.2806	3.149	1.7229	-0.7716	-0.2973	22	4.28	68.9
2012-10-10T05:49:34	132.5	32.7	26	0.0137	-4.3042	4.2905	-0.5896	0.4697	0.8573	22	4.37	80.9
2012-10-26T01:54:14	131.9	31.9	28	5.5318	-1.8796	-3.6522	3.7555	2.9964	-2.4523	22	4.51	74.9
2012-10-27T04:44:36	133.5	33.5	32	0.0585	-3.1104	3.052	2.0373	-0.4653	-0.1491	22	4.31	78.8
2012-12-22T15:15:29	132.3	33.6	44	-3.1873	0.2798	2.9075	0.0741	1.6438	-0.4459	22	4.3	74.7
2013-03-11T18:34:52	131.8	31.6	22	0.7453	-0.0027	-0.7427	0.5966	0.7457	-0.2558	24	5.33	74.6
2013-03-11T18:59:45	131.8	31.6	18	1.0296	-0.1435	-0.886	0.8015	0.9362	-0.2943	23	4.73	68.1
2013-04-13T05:33:18	134.8	34.4	14	3.5282	0.2016	-3.7298	0.1173	-1.9891	0.7873	24	5.68	86.6
2013-04-17T10:15:23	139.4	34.1	12	4.0018	1.2519	-5.2536	-3.6206	0.7026	-4.971	22	4.53	26.4
2013-04-17T11:13:58	139.5	34	6	0.6066	2.9894	-3.596	1.2982	-0.0078	-6.0277	22	4.5	62.6
2013-04-17T11:16:19	139.4	34.1	10	-1.5059	3.8416	-2.3357	-1.1352	-1.6548	-4.9695	22	4.47	32
2013-04-17T12:22:13	139.4	34.1	10	-0.0744	0.7911	-0.7167	-0.364	-0.2789	-0.9958	23	4.68	75.5
2013-04-17T17:57:37	139.4	34	8	0.2804	-1.7017	1.4213	-0.2263	-2.0019	-4.3235	24	5.73	78.3
2013-06-10T10:11:02	139.4	33.2	10	0.7045	-0.6324	-0.0721	-1.5068	0.7294	0.1011	22	4.1	41.5
2013-08-03T09:56:14	137.5	34.6	32	-1.8414	0.5047	1.3367	-0.2712	-0.2477	0.7867	23	4.78	78.6
2013-08-18T08:01:00	139.4	33.3	14	-0.2568	-0.014	0.2707	-0.1908	0.3922	-1.2715	23	4.69	67.5
2013-08-30T17:32:25	135.9	33.7	8	-1.7882	0.0163	1.7719	-0.1965	-0.5021	-1.8316	22	4.21	76.1
2013-09-28T04:37:48	131.5	31.2	28	1.4157	-1.101	-0.3147	0.1475	1.052	-0.7716	22	4.11	58.2
2013-10-08T20:45:22	131.9	31.8	20	3.3567	-0.682	-2.6747	3.0437	3.6202	-1.457	22	4.44	62.6
2013-12-12T11:25:14	131.2	31.2	30	-2.6186	0.3605	2.258	-2.6677	-3.857	-0.0001	22	4.42	48.1
2013-12-29T10:17:50	139.5	33.3	50	-2.3213	-0.2305	2.5518	-3.373	1.671	-6.9566	22	4.55	48.6

2014-03-13T07:35:54	131.4	31	26	3.1932	-0.7432	-2.4501	1.0824	0.8837	-1.5896	22	4.3	63.2
2014-04-04T00:46:43	132.1	32.5	34	-1.606	-0.0928	1.6988	1.7584	2.7185	0.7315	22	4.31	74.4
2014-05-29T09:18:00	139.4	33.3	14	-5.8398	2.8701	2.9697	1.5234	-0.5435	-3.0242	22	4.46	73
2014-08-29T04:14:36	132.1	32.1	22	2.385	-1.3919	-0.9931	2.3946	4.4971	-1.8215	24	5.78	82.6
2014-08-29T04:32:04	132.1	32.1	22	2.5535	-1.0894	-1.4641	4.1729	5.2609	-1.6985	22	4.51	45
2015-01-02T01:14:07	131.9	32.1	32	-0.5414	-0.1113	0.6528	0.444	2.4635	0.1783	22	4.21	79.5
2015-01-30T16:45:55	131.8	31.8	18	3.2694	-0.2876	-2.9817	2.9076	3.5835	-0.6984	22	4.43	64
2015-02-06T10:25:11	134.4	33.8	10	0.0838	0.8859	-0.9698	-0.1325	0.2548	-0.4568	23	4.62	86
2015-04-18T18:34:55	132.1	32	16	0.4897	-0.1686	-0.3212	0.5431	0.7164	-0.1401	23	4.6	70.7
2015-05-19T15:13:19	139.4	34.4	14	-0.3559	-0.6007	0.9565	-0.0486	0.0517	-4.184	22	4.35	70.4
2015-05-26T01:35:22	131.9	31.8	22	2.1759	-0.2887	-1.8872	1.5653	1.5741	-0.677	22	4.26	65.8
2015-06-06T16:28:13	139.3	33	10	-1.8498	-0.4521	2.3019	0.7025	2.7706	-4.5809	22	4.44	69
2015-07-13T15:52:35	131.8	31.4	28	-2.7135	-1.3844	4.0979	-0.2721	4.7081	1.8082	22	4.46	42.3
2015-07-15T16:18:47	139.2	33.2	12	0.3285	-2.1215	1.793	-2.7498	3.6604	-0.3661	22	4.4	44.7
2015-07-19T02:13:43	131.3	31.3	20	-1.066	0.2193	0.8467	-0.8225	-0.984	0.13	23	4.74	67.6
2015-07-24T17:53:34	132.4	33.4	40	-5.9261	-0.1244	6.0505	0.3362	4.3824	-0.2904	22	4.51	86.6
2015-08-21T16:54:35	132.2	33.3	44	-3.6329	0.5234	3.1095	1.6506	2.2531	1.1541	22	4.37	81.5
2015-08-26T07:51:36	131.9	32.1	34	-2.0236	-1.1574	3.181	2.4139	1.4665	1.3746	23	5.02	82.7
2015-09-02T16:07:47	134.6	33.3	12	-2.9105	1.6774	1.2331	-0.5466	1.9276	-1.7628	22	4.31	76.7
2015-09-08T20:22:39	138.4	34.7	18	0.894	-0.8622	-0.0318	1.2257	2.2265	4.1443	22	4.4	81.5
2015-12-25T11:20:36	134.5	33.5	32	-0.038	-2.4965	2.5345	-0.6622	0.5152	0.198	22	4.22	77.1
2016-04-01T11:39:09	136.4	33.4	10	3.2075	-1.9851	-1.2225	5.7603	7.4312	-1.554	24	5.93	80.8
2016-04-16T07:11:37	131.4	33.3	6	0.0122	2.6717	-2.6839	1.5596	1.1468	-1.4731	23	4.97	83.4
2016-04-16T14:03:56	131.2	33	6	0.3492	3.3242	-3.6734	0.3092	1.3586	-1.0284	22	4.33	71

2016-04-21T23:20:37	134.3	33.5	30	-0.5746	-3.3915	3.9661	0.4438	0.2301	-0.3544	22	4.32	76.5
2016-04-29T15:09:34	131.4	33.3	6	-0.1864	3.1013	-2.9149	1.0305	0.4916	-1.0067	22	4.29	63.2
2016-05-16T17:50:20	131.8	31.8	18	1.2032	-0.3495	-0.8537	1.0247	1.3676	-0.359	23	4.81	73.7
2016-07-11T15:22:01	139.4	33.3	14	-1.7994	0.5647	1.2346	0.6467	0.9714	-1.1017	23	4.84	80.3
2016-07-11T16:58:34	139.4	33.3	14	-4.0329	1.8471	2.1858	1.9735	1.2067	-1.9929	22	4.38	76.1
2016-07-11T17:33:02	139.5	33.2	10	-3.1075	1.7145	1.393	1.7574	1.019	-1.7902	22	4.32	58.8
2016-07-11T17:39:40	139.4	33.3	14	-1.9739	0.697	1.2769	1.2312	0.6247	-1.4048	22	4.21	61.5
2016-07-11T19:31:11	139.4	33.3	14	-2.7229	0.9532	1.7697	1.0057	0.9592	-1.3753	22	4.26	70.5
2016-07-12T05:54:20	139.5	33.3	14	-1.1808	0.384	0.7968	0.493	-0.1699	-0.6492	23	4.68	80.1
2016-07-12T06:56:52	139.4	33.3	12	-3.8721	0.6637	3.2084	2.2695	-1.0943	-2.4253	22	4.4	73.1
2016-07-12T07:34:02	139.4	33.3	12	-5.631	3.1221	2.5089	2.091	2.5566	-4.3533	22	4.51	75.4
2016-07-13T06:24:52	139.5	33.2	12	-2.541	1.4209	1.1201	1	0.6946	-1.727	22	4.26	57.3
2016-07-14T11:05:56	139.4	33.3	14	-0.9717	0.2777	0.694	0.8119	1.1479	-1.1006	22	4.13	20.4
2016-07-14T11:07:07	139.4	33.3	14	-3.3662	1.3522	2.014	1.5784	1.4813	-2.2552	22	4.35	49.9
2016-07-14T11:17:27	139.4	33.3	12	-3.9403	2.0106	1.9298	1.4	1.1681	-2.2075	23	5.03	80.3
2016-08-10T16:25:57	131.8	31.8	18	1.3331	-0.6217	-0.7114	1.2939	1.9569	-0.4921	22	4.22	69.6
2016-10-22T03:33:45	131.9	32.8	50	3.9676	-4.2294	0.2617	4.7291	3.137	-0.5439	22	4.5	83.1
2016-11-05T16:57:33	131.9	31.8	18	2.5509	-0.7718	-1.7791	1.9785	2.6455	-0.6888	22	4.34	73.6
2016-11-19T11:48:01	135.4	33.9	48	-3.6325	-4.0604	7.6929	2.7175	-0.4451	-5.7836	23	5.24	87.6
2017-02-07T16:21:51	131.5	31.5	18	-0.9278	0.9309	-0.0031	-0.566	-1.9684	0.0394	22	4.17	56.1
2017-02-08T03:19:27	134.6	33.4	32	-0.0637	-2.3988	2.4625	-1.0362	0.3671	-0.7235	22	4.23	77.8
2017-03-02T23:53:43	132.1	32.7	34	-3.5332	-0.7299	4.2631	1.5145	4.2689	0.786	23	5.12	79.7
2017-06-16T22:39:51	131.8	31.9	26	3.381	-0.6083	-2.7727	2.94	3.2205	-1.3037	22	4.43	80.1
2017-06-20T23:27:40	132	32.9	40	-0.4731	-0.1317	0.6049	1.2724	1.3717	0.6915	23	4.81	81.4

2017-07-02T00:58:22	131.3	33	10	-1.3107	2.2919	-0.9813	0.0344	-1.299	2.6235	22	4.3	79.7
2017-09-19T18:33:08	132.3	33.4	40	-2.5607	0.377	2.1837	0.0234	1.3128	-0.8112	22	4.24	78.7
2017-12-04T16:54:12	131.9	32.2	30	0.3743	-1.0503	0.676	0.7958	1.6386	-0.2401	22	4.14	80.7
2018-01-09T05:52:07	132.2	33.8	50	-2.3888	-1.4059	3.7947	0.6465	2.9379	-0.2507	22	4.37	75.8
2018-02-19T03:31:37	132.2	32.9	40	-2.8399	-0.5824	3.4224	1.7575	1.4811	-0.2862	23	5	84.7
2018-04-23T05:49:37	139.2	34.3	10	0.8199	-2.3806	1.5607	0.9054	0.2384	-0.7391	22	4.19	77.3
2018-04-28T13:27:34	131.9	32	6	-2.3439	0.0911	2.2527	-3.7815	-4.529	0.0852	22	4.47	68.7
2018-06-12T04:54:21	131.5	31.1	30	1.4716	-0.4028	-1.0688	0.6843	1.1412	-0.5431	24	5.46	74
2018-10-04T17:20:53	131.2	31	30	5.9256	-3.3772	-2.5483	2.2505	4.7264	-2.2398	22	4.52	68.2
2018-11-02T16:53:54	135.2	33.7	40	-0.4302	0.035	0.3952	0.2262	-0.6334	-0.8114	24	5.3	89.3
2018-11-05T08:19:14	135.3	33.7	46	-0.6427	-4.0587	4.7014	2.194	-1.7504	-4.0383	22	4.48	81.7
2019-01-21T23:17:08	132.4	32.9	28	0.0401	-1.7516	1.7115	-0.2722	0.271	0.3018	22	4.1	74.6
2019-03-11T15:37:49	132.7	33.2	34	-0.3189	-0.8166	1.1355	0.3179	0.2012	-0.5394	23	4.65	79.2
2019-03-13T13:48:47	134.9	33.8	38	0.5685	-5.9744	5.4058	-0.8286	-1.857	-1.6438	23	5.13	84.2
2019-03-27T09:11:23	132.1	32.1	22	3.5887	-1.6418	-1.9469	3.2572	6.4347	-2.7917	23	5.21	83.7
2019-03-27T15:38:04	132.1	32.2	22	3.8583	-1.2031	-2.6552	4.6751	7.613	-2.3919	23	5.26	84.5
2019-04-23T07:49:50	131.2	31.3	24	-1.4358	0.4849	0.9509	-1.2569	-2.2809	-0.0562	22	4.24	73.1
2019-05-10T07:43:24	131.9	31.8	20	2.4441	-0.6387	-1.8054	2.1455	2.7885	-0.7343	24	5.68	73.1
2019-05-10T08:48:46	131.8	31.9	26	1.0889	-0.1965	-0.8924	1.1381	1.5277	-0.4371	25	6.16	80.1
2019-05-10T09:07:37	131.9	31.8	26	2.005	-0.0686	-1.9364	0.9407	0.9768	-0.1032	23	4.85	50.8
2019-05-10T13:53:53	131.9	31.8	22	1.9288	0.4866	-2.4154	2.0226	1.1028	-0.8503	22	4.28	47.8
2019-05-10T20:40:38	131.8	31.8	28	4.575	-2.3805	-2.1945	2.6548	5.059	-2.0404	22	4.51	77.6
2019-05-11T08:59:39	132.3	32.7	32	-0.7341	-0.2024	0.9365	0.3296	1.3177	-0.1167	23	4.74	87.8
2019-05-12T15:07:42	132.3	32.7	32	-1.6641	-0.1141	1.7782	0.2608	1.938	-0.0225	22	4.21	77.1

2019-06-19T11:35:45	131.2	31	32	2.5038	-1.4996	-1.0042	1.1971	2.9308	-0.7981	22	4.33	58.6
2019-07-27T02:11:47	131.8	31.6	24	1.7323	-1.5534	-0.1789	1.4295	2.5845	-1.4655	22	4.31	80
2004-04-20T22:26:31	132.3	33.5	38	-1.357	-1.6975	3.0545	-2.4812	-1.2316	1.3686	22	4.34	67.5

Table S2. CMT solutions for the *Mw* 7.2 and 7.5 earthquakes.

Centroid time (JST)	Lon.	Lat.	Depth [km]	M_{rr}	$M_{\theta\theta}$	$M_{\phi\phi}$	$M_{r\theta}$	$M_{r\phi}$	$M_{\theta\phi}$	Exp.	Mw	VR [%]
2004-09-05T19:07:13	136.7	33	26	3.4335	-4.5007	1.0672	-0.1465	0.4235	0.4357	26	7.01	70.9
2004-09-05T23:57:42	137	33.2	20	0.8675	-1.1077	0.2402	-0.3706	0.1465	0.1220	27	7.29	71.8